Lappeenranta- Lahti University of Technology
LUT School of Engineering Science
Degree Program of Chemical Engineering

Master's Thesis
2021

Zubair Riaz

MODELLING OF GAS SEPARATIONS USING ASPEN ADSORPTION® SOFTWARE

Examiners: Docent Arto Laari
Professor Tuomas Koiranen
Supervisors: Docent Arto Laari
M.Sc. Pavel Maksimov

ABSTRACT

Lappeenranta- Lahti University of Technology

LUT School of Engineering Science

Degree Program of Chemical Engineering

Zubair Riaz

Modelling of gas separations using Aspen Adsorption ®software

Master's Thesis

2021

74 pages, 44 figures, 26 tables, 01 appendix

Examiners: Docent Arto Laari

Professor Tuomas Koiranen

Supervisors: Docent Arto Laari

M.Sc. Pavel Maksimov

Keywords: Gas separations, Aspen Adsorption, simulation, modelling, CO_2 capture and utilization

Gas separation is an important and extensively studied topic in chemical and process engineering. Its importance comes from the fact that almost all the manufacturing processes involve separation at some point in the process and separation adds to the major cost of the complete process. Capture and removal of some gases, such as carbon dioxide, and water, is important when CO_2 emissions are reduced, and the captured CO_2 is utilized.

This study focused on finding the right tool for modelling and simulation of adsorption processes. For this purpose, a flowsheet simulator by AspenTech called Aspen Adsorption® was used to understand and evaluate its capabilities.

A comprehensive literature review was conducted in Chapters 2 and 3 to understand how to separate gases and why adsorption is in some cases a useful process. These chapters discuss in detail the need to capture CO_2, the different methods available for separation, adsorption processes, and adsorption materials available. The phenomenon of adsorption is understood

through isotherms, and they are also briefly explained here. Finally, the modelling of the adsorption process was analyzed to understand the mathematical equations that govern the model for the simulations.

Before the practical part, a short chapter is included to get the idea of the user interface, available options, and a general guide about setting up the simulation in Aspen Adsorption®.

Several cases and configurations were considered for the simulation. The first case is a simple once through adsorption case for nitrogen and oxygen separation. The second case is for the separation of methane and carbon dioxide from biogas. The third case is the cyclic set up of the biogas case involving a TSA to simulate adsorption and desorption cycles. The last case is to check the capabilities of the software for the adsorption of water.

Aspen Adsorption® was found to be a comprehensive tool for the modelling and simulation of simple adsorption processes, as well as the cyclic processes. Flowsheet setup is rather simple and straightforward, but interpretation of warnings, errors and some results might be hard to comprehend for an inexperienced user. It was found that the setup of the Cycle Organizer is complicated and some training and support from the software manufacturer would be useful to set up the Cycle Organizer correctly.

Table of Contents

Acronyms

BET	Brunauer-Emmett-Teller
BTC	Benzene-1,3,5-tricarboxylate
BUDS	Biased upwind differencing scheme
CCS	Carbon capture and sequestration
CCU	Carbon capture and utilization
CDS	Central differencing scheme
DAC	Direct air capture
ESA	Electric swing adsorption
HKUST	Hong Kong university of science and technology
IGCC	Integrated gasification combined cycle
IPCC	Intergovernmental panel on climate change
IUPAC	International Union of Pure and Applied Chemistry
LDF	Linear driving force
LDS	Leonard differencing scheme
LUT	Lappeenranta-Lahti University of Technology
MEA	Monoethanolamine
MOF	Metal organic framework
MTC	Mass transfer coefficient
ODE	Ordinary differential equation
PDE	Partial differential equation
PSA	Pressure swing adsorption
QDS	Quadratic differencing scheme
TSA	Temperature swing adsorption
UDS	Upwind differencing scheme
VOC	Volatile organic compound
VPSA	Vacuum pressure swing adsorption

Nomenclature

b	Langmuir parameter, bar $^{-1}$
b_0	Adsorption affinity at infinite temperature, bar $^{-1}$
b_T	Adsorption affinity, bar $^{-1}$
c	Parameter related to heat of adsorption
C	Concentration, mol m^{-3}
$C_{p,g}$	Heat capacity, J K^{-1}
d_p	Diameter of the particle, m
D_{ax}	Axial dispersion coefficient, m^2 s^{-1}
D_M	Molecular diffusivity, m^2 s $^{-1}$
h_{in}	Heat transfer coefficient, W m $^{-2}$ K $^{-1}$
IP	Isotherm parameter
j	Heterogeneity parameter, kmol kg $^{-1}$
K_{ax}	Thermal conductivity, W m $^{-1}$ K $^{-1}$
k_F	Freundlich constant, kmol kg^{-1} bar $^{-1}$
M_r	Molecular weight, kg/kmol
p	Pressure, bar
p_i	Partial pressure of component i, bar
p_{sat}	Saturation pressure, bar
$\frac{p_i}{p_{sat}}$	Relative pressure
q	Adsorption capacity, kmol kg $^{-1}$
$\bar{q}$	Average transient adsorbent loading, kmol kg $^{-1}$
q_0	Amount adsorbed at saturation, kmol kg $^{-1}$
q_e	Equilibrium adsorbent loading, kmol kg^{-1}
$\overline{q_1}$	Average solid loading, mol kg $^{-1}$
q_m	BET monolayer capacity, kmol kg $^{-1}$
q_s	Maximum adsorption capacity, kmol kg $^{-1}$

r_{in}	Internal radius, m
r_p	Radius of the particle, m
R	Universal gas constant, kJ mol $^{-1}$ K^{-1}
Re	Reynolds number
t	Time, s
T	Temperature, K
T_s	Saturation temperature, K
T_w	Temperature of the wall, K
v	Interstitial fluid velocity, m s $^{-1}$
v_g	Velocity of gas
z	Length along z direction, m
n_F	heterogeneity factor
ΔH	Heat of adsorption, kJ mol $^{-1}$
ε	Bed void fraction
μ	Gas viscosity, Pa s
ψ	Shape factor
ρ_g	Density of gas, kg/m^3

1 INTRODUCTION

There has been an increase of more than 1 °C in global average temperature since pre-industrial times [1]. Some areas have seen more increase in the temperature than the others. This rise in temperature is termed as global warming, and it is primarily the result of human activities.

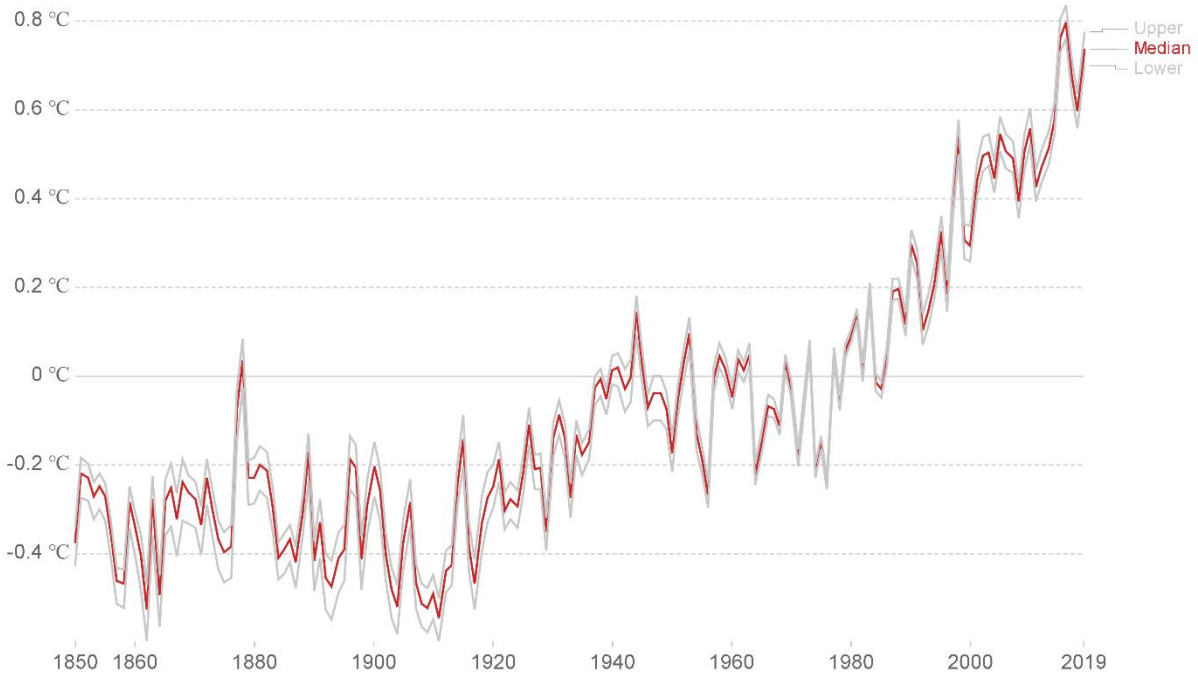

Figure 1. Global average temperature anomaly relative to 1961-1990 average temperature [1], [2]

When we look at the red line in Figure 1, we observe a rapid increase in temperature since 1980s compared to the 1961-1990 average temperature. More importantly, before 1870 the temperature was colder than the average temperature. So essentially since 1850s temperature has risen more than 1 °C in 2019.

Climate change is the adverse effect of global warming, and it can change the way of life as we know it today. This change can disrupt not only the lives of human beings but also of all the other living organisms. One most commonly observable change is the increase in heatwaves across both the land and the oceans. Moreover, it causes changed patterns in both amount and frequency of the precipitation. In case of heavy precipitations, it is possible to face flash floods that could be devastating. On the contrary, it can cause droughts in other parts especially in the Mediterranean region [3].

This change would be even worse if this temperature surge reaches 2 °C and more. Scientists predict that this would cause coastal regions to suffer a lot. This would come in shape of storms

and floods, and as previously mentioned further increase in droughts. The sea water could become acidic that would result in extinction of the coral life. Beyond the arctic circle, life of polar bears is already affected, and with melting ancient ice sheets means that many species could go instinct. These ancient ice sheets reflect the sunlight, with them melting temperature would rise further. Moreover, this could lead to a lower number of rainforests, eventually forcing many species to go extinct, and for humans it means displacement in huge numbers [4].

These catastrophic affects are because of the human activities, particularly the combustion of fossil fuels. Greenhouse gasses are released because of the burning of these fossil fuels, that in turn contributes to the global warming. Most common greenhouse gases are water vapors, carbon dioxide, methane, chlorofluorocarbons, and nitrous oxides.

A certain amount of CO_2 is essential to maintain a livable temperature on earth by acting as a blanket to trap heat, but too much of it is a problem. Since we have already established that human activities are the major contributor of the greenhouse gases this gives us an opportunity to reduce the release or use them in innovative ways to protect our environment.

CO_2 is the major contributor amongst the greenhouse gases that result in the climate change. The primary source of the environmental CO_2 is the combustion of the fossil fuels [1]. These fuels are used by numerous sectors including but not limited to electricity, heat production, major chemical and metallurgical industry, transportation, forestry, and agriculture. As of 2018, 81.3 % of these CO_2 emissions comes from these sectors [5].

Figure 2 clearly shows that as the emissions increased over the last century, so did the atmospheric concentration of CO_2. The concentration reached more than 410 ppm. This graph is analogous to Figure 1, clearly showing the relation of CO_2 levels to the global average temperature. The higher the CO_2 the higher the temperature and vice-versa.

Now that we have recognized that reducing the CO_2 is of the utmost need, we now look at some of the ways we can do that.

Most agreed upon way is to cut out the need for fossil fuels and move towards green solutions for transportation, heating/cooling, and electricity production. With recent progress in development of electric and hybrid vehicles, solar energy, and wind energy this could greatly help control the further increase in these levels.

Furthermore, conservation of energy, utilization of more efficient systems, and using alternative fuels could also help to some extent [5]. However, the transition period towards these methods is protracted and we need to compliment these technologies to achieve this goal. For this we look further into carbon capture and separation methods.

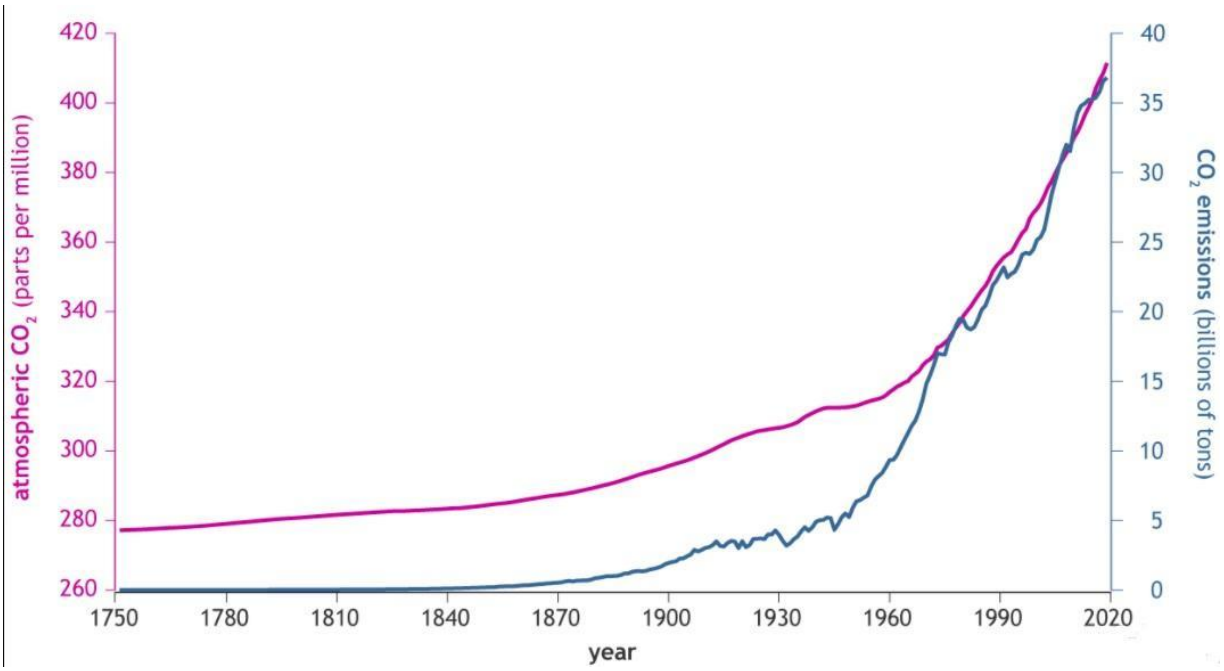

Figure 2. Yearly trend of CO_2 emissions and atmospheric levels [6]

CO_2 can either be captured and stored (CCS) or captured and utilized (CCU). CO_2 can be captured in two different ways. It can either be captured from the point of release such as flue gas streams or directly from the air (DAC), depending on the application.

There are several technologies that can be used to capture carbon dioxide. One of the most well-established method is absorption of CO_2 from the mixture of gases into absorbent solution such as monoethanolamine (MEA). After capturing, the desired gas is desorbed from loaded solution, in this case pure CO_2 for further use or storage.

Another method for CO_2 capture is called adsorption. This is when a gas is adsorbed on the surface of a solid adsorbent. Adsorbent is commonly used in a fixed bed type contactor, and adsorbent materials include activated carbon from different sources, zeolites, metal organic frameworks, hydrotalcites, and more.

Other methods include membrane separation, and cryogenic distillation, but adsorption is the focus of this study.

There are numerous ways in which this captured CO_2 can be utilized. It has applications in many sectors such as food and beverage, pharmaceuticals, chemicals, environment, metals industry, safety, healthcare, and chemicals industry [7].

In chemical industry CO_2 is used in synthesis of numerous products. It is used to produce urea, dimethyl carbonate, salicylic acid, acetic acid, carbon monoxide for syngas and other hydrocarbons are produced by reaction with H_2 [8].

In many of these processes water is produced as a byproduct, that reduces the equilibrium yield of the products. Therefore, in-situ removal of H_2O greatly enhances the performance of the synthesis process. Sorption-enhanced synthesis has been proposed as a potential method to improve yields in methane and methanol production. The principle is that equilibrium is shifted towards products when H_2O is separated from the product stream [9].

Adsorption process such as temperature swing adsorption (TSA), and pressure swing adsorption (PSA) are transient in nature, that means process is continuously shifted between adsorption and desorption cycles. This means that the optimal design of such a system is a major engineering challenge.

For design of such a transient system, this study proposes a use of a commercial software to carry out simulation and optimization tasks. One such software is Aspen Adsorption® that has emerged as a potential and useful tool for the design of adsorption processes.

1.1 Objectives

The main objective of this study is to contribute towards the carbon capture and utilization techniques to reduce the amount of CO_2 in the environment. We propose to do that by simulation and design of proper adsorption processes related to different streams containing CO_2 or water as a reaction side product. The case studies include direct air capture and separation, capture from point sources, and removal of water from process streams. The simulation software chosen is Aspen Adsorption®. This particular software is chosen to understand its suitability for industrial processes involving adsorption.

LITERATURE REVIEW

2 CO_2 CAPTURE AND SEPARATION TECHNOLOGIES

Carbon dioxide capture technologies usually refers to the stage and the process from where the CO_2 is being separated from. It can either be pre-combustion carbon capture, oxy-combustion carbon capture or post-combustion carbon capture [10].

In pre-combustion carbon capture, as the name suggests the carbon is removed before the complete combustion itself. According to IPCC's special report [11], pre-combustion carbon capture results in the production of synthesis gas (syngas). This is achieved by reacting a fuel with air or oxygen, and/or steam. This technology is commonly applied to integrated gasification combined cycle (IGCC) power plants [12]. These reactions are given in Equations 2.1 and 2.2 [13].

$$C_xH_y + xH_2O \leftrightarrow xCO + (x + y/2)H_2 \Delta H_{CH_4} = 206 kJmol^{-1} \quad (2.1)$$

$$C_xH_y + \frac{x}{2}O_2 \leftrightarrow xCO + (y/2)H_2 \Delta H_{CH_4} = -36 kJmol^{-1} \quad (2.2)$$

The syngas is a mixture of hydrogen and carbon monoxide. Further, even more hydrogen is produced when carbon monoxide is subjected to a reaction called a shift reaction (Eq. 2.3) [13]. In shift reaction carbon monoxide is reacted with steam to give off hydrogen and carbon dioxide. It is at this point that CO_2 is separated out.

$$CO + H_2O \leftrightarrow CO_2 + H_2 \, \Delta H = -41 kJmol^{-1} \tag{2.3}$$

Usually, CO_2 is given off at a high pressure from the water-gas shift reaction, therefore, it is relatively simple to capture and separate it. CO_2 is usually separated using industrially mature technologies such as physical and chemical absorption, and membrane separation [12]. Apart from this advantage, we get a clean fuel in form of hydrogen.

For the oxy-combustion carbon capture, oxygen with purity greater than 95% is used instead of air for the combustion. The problem with this technique is the high cost related to the supply of pure oxygen. Furthermore, it is not technologically ready at this point.

Post-combustion capture involves capture of carbon from flue gas streams. The main components of flue gasses from power plants includes carbon dioxide and nitrogen. One of the main contributors to the cost is the need of compression after capturing the CO_2 since, CO_2 evolves at rather low pressures in post-combustion capture [10]. In case amine sorbents are used their regeneration also is a major factor for cost [10]. Since flue gas contains small concentrations of carbon dioxide, large amounts are required to be treated. However, this technology is the easiest to integrate with the current plant setups. Even for the maintenance the plant is not required to be shutdown.

There are a few established methods used to separate CO_2 either directly from the air or from the different gas streams. These methods include physical absorption, chemical absorption, membrane separation, cryogenic separation, hydrate separation, and adsorption [14]. It is also worth noting that physical and chemical absorption can work in a combination [15].

2.1 Physical absorption

Physical absorption is a very popular method when it comes to separation processes. This process works on the principles of Henry's law [16], [17]. For this process a solvent is used to physically absorb CO_2 [17]. This method works best when the temperature is kept low and the pressure high. This is because physical absorption is solubility-based phenomenon, and it works best at the mentioned conditions. Moreover, this method is energy efficient only if the partial pressure and the concentration of the desired gas to be separated is high in the feed stream [15].

Typically, the solvents used are not corrosive and they are not toxic in nature. Some of the solvents used are water, propylene carbonate, methanol, normal methyl pyrrolidone, tributyl phosphate, dimethyl ether of polyethylene glycol, and a mixture of polyethylene glycol dialkyl ethers [15].

Power demand for the regeneration of this process is high in case thermal regeneration is used. Otherwise, compressing the feed gas to a high pressure is the most energy demanding step of the process [15].

2.2 Chemical absorption

This is another well-established and studied method for the absorption of CO_2. Since it involves a chemical reaction to capture CO_2 it is also known as reactive absorption. In addition to a reaction, absorption process also involves absorptive mass transport.

The most mature solvent is an amine-based solvent called Monoethanolamine. Apart from amine-based solvents, different carbonates, ionic-liquids, and aqueous ammonias are also used as absorbents [18].

Contrary to physical absorption, regeneration is the most energy intensive step involving high temperature. Heating enables the intermediate compound that is weakly bonded to be released from the solvent [19].

2.3 Membrane separation

Generally, a membrane is a solid film, and sometimes it can be a fluid film of a small thickness. This method of separation works because of a physical or chemical interaction between a certain gas and the membrane material. Chemical potential gradient is the driving force for the movement across the membrane. The membrane material and its structure determine the flux. Separation by membranes is classified by the driving force and the pore size. Some of these classifications are microfiltration, ultrafiltration, nanofiltration, reverse osmosis, and ion-exchange [20].

There are quite many applications for membrane separation of gases, including air separation of nitrogen and oxygen, purification of medical grade oxygen, water removal, purification of natural gas by capturing CO_2 and H_2S, removal of volatile organic liquids, separation of hydrogen from multiple different streams and plants, separation of methane from biogas, syngas separations, and nitrogen enrichment for inerting systems [20].

Two main classes of membrane materials are organic polymeric membranes, and inorganic membranes. The polymeric membranes are further divided into glassy and rubbery polymers, though glassy polymers change to rubbery when heated to a certain temperature.

Glassy polymers are rigid in nature, have high selectivity with a moderate permeability. Lower free volume results in the high selectivity of glassy polymers. Some examples of commercially available glassy polymers for gas separations are polyamides, polyphenylene oxide, cellulose acetate, and polysulfone [20].

Rubbery polymers possess low selectivity with high permeability. One such commercially available material is polydimethylsiloxane.

There are several factors to consider for successful application of membrane separation. For the membrane to work, a pressure difference is to be maintained across the membrane. This allows a high permeability gas to pass through, and gases with low permeability are held back. Therefore, feed should be available at suitable pressure, that is usually high. High recovery purity is not always possible, so applications where moderate purity is required can be considered. Moreover, selectivity is important for successful separation. Feed should not contain harmful substances that can damage the membrane. The component to be concentrated should be available in large amounts [20]–[22].

One major advantage of membrane separations is its simple set-up and operation. Other advantages are ease of scalability due to modular design, no phase change involved, no need for chemical additives, possibility of recycling, and the continuous steady-state operation [20].

On the other hand, there are several challenges of using membranes. Membranes are prone to fouling and cake formation, resulting in decline of performance over time. Concentration polarization is another problem, though not very noticeable for gas separation. Fouling problem can be solved by cleaning and purging with gasses that do not adsorb. Prefeed filters can also be used to avoid it to a certain level. Due to high pressure, pore size can reduce in polymeric membranes by the phenomenon known as compaction.

Maintaining pressure is the only high energy demanding step. Since most flue gases contain a minor amount of CO_2, the residence time is high. This means that process needs to run for a long time adding to the cost. The membrane needs to be highly selective for CO_2 in order to be useful for the industrial scale separation [21].

Furthermore, the membranes are made such that they cannot handle temperatures above 100° C, therefore flue gases are required to be cooled before they are passed through membrane. Adding an additional step. Although ceramic membranes are available that can handle high temperatures, it is extremely difficult to make them of the right thickness without cracking the material [23]. The available ceramic membranes are expensive and exhibit low selectivity towards CO_2 [23]. Moreover, membranes must be corrosion resistant to survive harsh chemicals present in flue gases. Few of the membrane materials with high selectivity for CO_2 are different polyamides, polyethylene oxide, mixed matrix membranes involving inorganic materials, and carbon molecular sieves [21], [24].

This method can be considered as one of the least expensive and energy intensive process of all the mentioned processes. Although, the effectiveness of the membrane decreases with time [25].

2.4 Cryogenic distillation

This method consists of some of the most fundamental processes related to chemical engineering. This process involves getting the temperature of the feed stream as low as -80° C so that CO_2 is condensed and recovered in its liquid form. Therefore, it involves refrigeration, compression and separation steps [26]. These steps are very well established that makes this separation process industrially operational.

However, there is a possibility of frost formation at such low temperatures, that imposes a risk for the safety of equipment. Maintaining this kind of temperature is also not economically feasible. This process requires a lot of integration and optimization to make it feasible [26].

2.5 Adsorption

In the process of adsorption, the gas or liquid molecules, ions, or atoms are diffused from the bulk fluid stream to the surface of a solid adsorbent. The adsorbed species known as adsorbate is attached to the adsorbent by weak intermolecular forces. The weak forces can be recognized as the van der Waals forces [27]. The forementioned method of adsorption with weak forces is known as the physisorption. Another type of adsorption is known as the chemisorption, where the binding force is the stronger covalent bond [28]. It is important to notice that adsorption is a surface phenomenon.

2.6 Comparison of the separation technologies

Table 1 gives the comparison for all the previously mentioned separation techniques. Wherever possible, advantages, drawbacks, and the energy consumption is given.

Table 1. Comparison of separation technologies

Technology	Advantages	Drawbacks	Energy Consumption	References
Physical absorption	● Well established method with several commercial processes. ● CO_2 can be removed at low temperature. ● Low toxicity. ● Lower vapor pressure. ● Solvent less corrosive.	● High energy cost related to compression of feed gas.	Theoretical energy including recovery = 1.4 GJ/t CO_2	[16], [29]
Chemical absorption	● Most mature for CO_2 capture and commercialized. ● Can be utilized with current industrial set-ups.	● Better absorbent efficiency required. ● Improvement required for overall process. ● Low CO_2 capacity. ● Results in equipment corrosion. ● Amine absorbent degraded by several flue gas components. ● High energy demand for regeneration. ● Large equipment.	Theoretical energy including recovery and compression of CO_2 to 150 bar = 0.396 GJ/t CO_2 Practical energy consumption expectation= 0.72 GJ/ t CO_2	[16]

Continuation of Table 1.

Membrane separation	● Membranes much more stable than they used to be.	● Low selectivity ● Product purity is of not the desired level with single run of the process. ● Compression required for enough driving force	Theoretical energy consumption = 0.5-1 GJ/t CO_2	[22], [30]
Cryogenic distillation	● Simple and well-established. ● New method using cold $N_2$from nitrogen removal unit, takes away the need of separate refrigeration. ● Production of highly pure liquid CO_2 possible. ● Moderate pressure requirement.	● Operating cost is high.	Theoretical specific energy consumption = 0.425 GJ/t CO_2	[26], [30]
Adsorption	● Energy efficient ● Ease of regeneration by varying the temperature and pressure. ● Range of materials available. ● Relatively new approach means room for improvement.	● Work required to improve stability and performance of adsorbent materials. ● Small difference in size of gas molecules makes separation difficult for some mixtures. ● Low selectivity. ● Presence of H_2O lowers the capacity for CO_2. ● Not suitable for post-combustion capture.	For TSA, specific energy consumption = 3.23 GJ/t CO_2. For ESA, specific energy consumption = 4.08 GJ/t CO_2. For modified 7 step ESA, Specific energy consumption = 1.9 GJ/t CO_2.	[10], [16]

3 ADSORPTION THEORY

Adsorption is strictly a surface phenomenon where ion, atoms or molecules are adhered to the surface of the material being used. The specie attaching itself is called the adsorbate, and the material used for this purpose is called the adsorbent. This process works for separation based on the differences in adsorption and desorption of the involved species. When an adhered specie leaves the surface of a material it is called as desorption [10].

The attraction between the adsorbate and adsorbent is either based on the physical interactions or covalent bonding. Physical interactions are usually weak van der Waals forces and such mechanism of adsorption is referred as physisorption. Chemisorption is the term used for when mechanism involves covalent bonding or electrostatic attraction [10].

3.1 Adsorption materials

The adsorbent is considered ideal if it is highly selective for CO_2 and it has a high adsorption capacity. Moreover, it should not attach with CO_2 too strongly, else it would require a lot of energy to regenerate. It is also important that adsorbent is selective even at different temperature and pressure conditions. For physical adsorption, factors that are considered while evaluating a adsorbent are pore size and volume [31].

3.1.1 Activated Carbon

It is one of the most complex adsorbent materials available in the industry, and it has desirable properties as an adsorbent. It has very high micropore volume and a suitable pore size distribution. Also, the surface area is extremely high, enabling it to be used in various applications [31], [32]. Furthermore, activated carbon is not ruined by water due to its hydrophobicity, is highly stable at high temperatures, and it is resistant to different chemical environments [33].

Different carbon containing materials can be converted to porous carbon structure, and then they are activated either physically or chemically to get a suitable activated carbon adsorbent. Physical activation is achieved by using an oxidizing agent such as steam, air, or carbon dioxide. Chemical activation is preferred since it allows achieve better pore structure, but chemical used needs to be washed off, adding an extra step. Typical chemicals used are zinc chloride, potassium chloride, potassium hydroxide, and phosphoric acid [34]–[36].

Common sources for carbon are petroleum pitch, coal, wood, peat, sawdust, bamboo, and some other more recent discoveries.

Activated carbon does not perform well when temperatures are above 250° C, but still is suitable for most flue gas temperatures [31].

3.1.2 Zeolites

Zeolites are one of the most used materials for the adsorption processes. One zeolite type, 13X is a kind of adsorbent used for benchmarking (against which the other adsorbents are compared to). They are suitable to adsorb CO_2 at high pressures and they can withstand high temperatures

of regeneration. For zeolites to perform well elevated temperature is needed to remove moisture because they do not perform well when moisture is present [28]. Although, in absence of moisture they perform the best at high pressures and low temperatures. There adsorption capacity ranges from 0.15 to 5.5 mol/kg [37]. Zeolites can selectively adsorb CO_2 out of the flue gasses [38]. It is possible to perform adsorption at the room temperature and for desorption, temperature needs to be risen to 120° C for the zeolites. Common types of zeolites are given in Table 2.

Table 2. Chemial formulas and compositions of common zeolites [38]

Zeolite type	**Chemical formulas**	**Composition (wt %)**					
		Na	**Al**	**Si**	**Ca**	**K**	**Mg**
13X	$5Na_2O•5Al_2O_3•14SiO_2•XH_2O$	11.7	14.2	18.2	0.5	0.2	1.2
4A	$Na_2O•Al_2O_3•2SiO_2•XH_2O$	10.8	13.6	16.1	0.8	0.9	1.2
5A	$0.7CaO•0.3Na_2O•Al_2O_3•2SiO_2•4.5H_2O$	3.8	14.8	16.7	7.8	0.8	1.0
WE-G 592	Sodium form X crystal structure, sodium aluminosilicate	13.7	15.6	16.5	0.1	0.1	ND
APG-II	Sodium form of type X molecular sieve, $Na_x[(AlO_2)_x•(SiO_2)_y]•z\ H_2O$	8.8	10.7	14.3	0.5	0.2	1.0

Zeolite 13X is of a crystal type with a uniform aperture. Silicon oxygen tetrahedron with oxygen bridges and alumina tetrahedra make up the structure of zeolite 13X [39]. The β-cages are the basic building block of the whole structure, and they join to make the molecular sieve by hexagonal prism connections. SII and SIII are the only available sites for the adsorption [39]. The structure is shown in Figure 3.

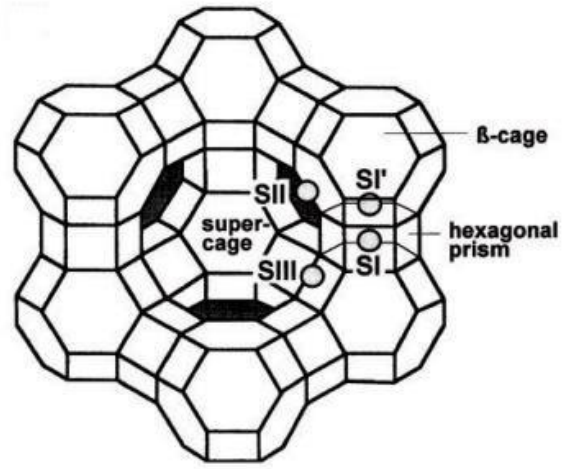

Figure 3. Structure of zeolite 13X [39]

Zeolite 4A contains both the alpha and beta cages. The structure is made up of eight α and βcages each. The effective pore size in zeolite 4A is reduced due to the presence of charge balancing cation Na by 1 or 2 Å [40]. The α and βcages connect with each other with hexagonal rings, and the βcages are connected to each other with the four membered rings. The structure of zeolite 4A is shown in Figure 4. Oxygen in the structure is shown in red, silicon in yellow, sodium in green, and aluminum in purple. Structure of other A type zeolites is the same with different pore size and chemical composition.

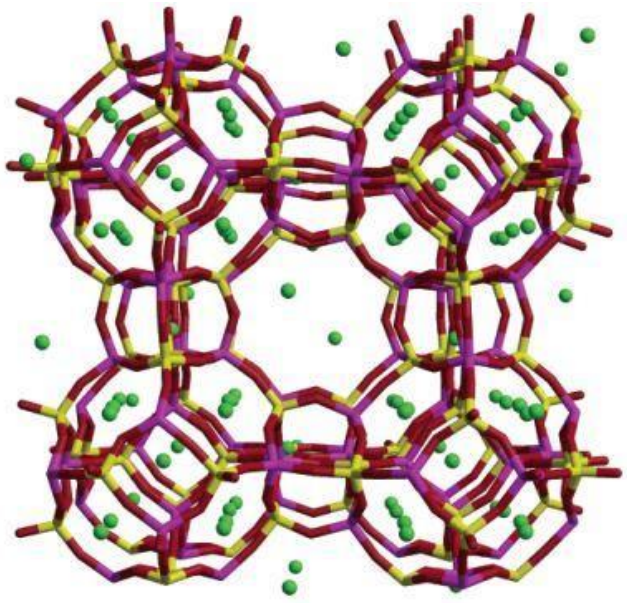

Figure 4. Structure of zeolite 4A [40]

3.1.3 Metal Organic Frameworks (MOFs)

MOFs are the latest materials introduced for adsorption and a lot of recent research is focused on them. These materials are coordination polymers that have crystalline structure and are made of metal containing nodes joined by organic ligands [28], [41], [42]. The metals usually used are nickel, magnesium, cobalt, and zinc. Other metals such as aluminum and chromium have also been used. For ligands, there are numerous possibilities from the organic compounds.

MOFs are microporous in nature. Properties of MOFs can be tailored according to the needs of the process. These properties are dependent upon the process of manufacturing, the chosen material, and the modifications to the product that are achieved synthetically.

MOFs can be considered ideal in many ways when it comes to CO_2 capture. It has a higher porosity compared to the other materials, and a higher specific surface area [43]. This in turn allows for a higher uptake of the gas being adsorbed. Moreover, the process of adsorption itself is faster in MOFs. Some even have higher selectivity than zeolites and activated carbons. One such example is of Hong Kong university of science and technology -1(HKUST-1) MOF, whose chemical formula is $[Cu_3(BTC)_2(H_2O)_3]$. Furthermore, these properties can be further improved by doping and post-synthesis techniques.

On the other hand, all MOFs might not work well when water is present. Some materials perform well with water but then again it might have lower selectivity for other gas combinations. Also, they might only be suitable for PSA since they are not very hydrothermally stable. Still, a lot of work is required to get the ideal adsorbent with competitive price.

3.1.4 Hydrotalcites

Hydrotalcites are classified as anionic clays. They are commonly manufactured by the method of co-precipitation, while precipitation of hydrotalcites assisted by microwaves and ultrasound tend to show better surface properties [44]. These novel methods of sorbent preparation give 2-5 times higher surface area that further translates into higher adsorption capacities.

These materials are suitable for high temperature CO_2 adsorption. They show breakthrough capacities of 1.6 mmol CO_2/g of sorbent at temperature of 350 °C and 13 bars pressure. Such temperature conditions are present for gasses after water gas shift reactions, making these materials suitable for pre-combustion capture of CO_2 from coal fired power plants.

Temperature needs to be risen to 470 °C for the TSA regeneration.

Hydrotalcites have a layered structure, with each layer composed of double hydroxides. Between the layers are the interchangeable anions [45]. The multilayers of hydrotalcites provide large surface area for the adsorption. The structure is shown in Figure 5.

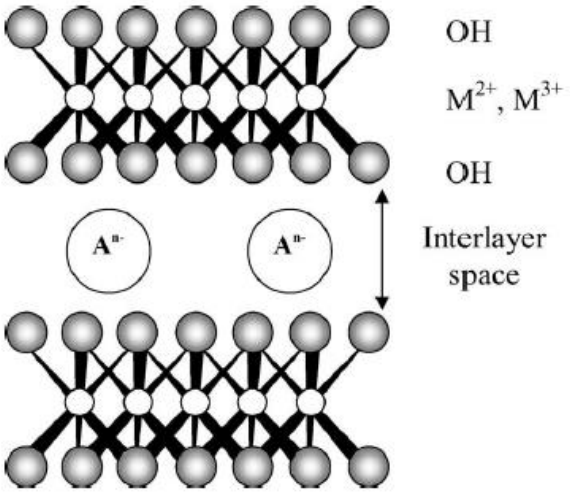

Figure 5. General structure of hydrotalcites [45]

3.2 Adsorption isotherms

The adsorption isotherms help understand the pore structure of the solid adsorbent, uptake of adsorbate at equilibrium is visualized, and provides enough information to calculate and design the process of adsorption [46]–[48].The most common type found in the literature is the Langmuir isotherm, and it further provides basis for the other types of available isotherms [49].

3.2.1 IUPAC's classification for isotherms

International Union of Pure and Applied Chemistry (IUPAC) has classified adsorption isotherms in six different types. Four of them are reversible, and two follow different paths for adsorption and desorption. All six types show distinct shapes of isotherms [48], [50]. Figure 6 shows all these shapes.

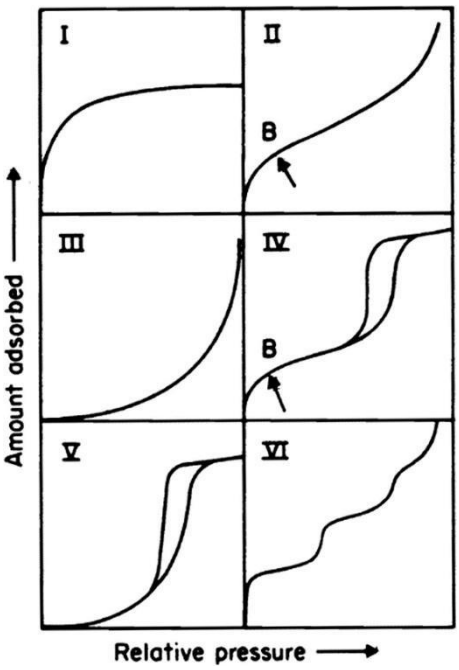

Figure 6. Six IUPAC shapes for adsorption isotherms [50], [51]

Most common types are types I, II, and IV. Type-I is exclusively for the microporous solids with their external surface being comparatively small. This reversible isotherm shows higher initial uptake and then the curve quickly flattens towards the saturation point. Certain sorbents made from activated carbons, and zeolites give such isotherms [50].

Type-II is for monolayer and multilayer adsorption on nonporous or macroporous solids. Point B shows the point at which multilayer adsorption begins after monolayer adsorption is complete. This also shows that major portion is for multilayer adsorption, and unlike type-I, adsorption continuously increases with increase in pressure [50].

Type-III is not so common but still found for some systems such as nitrogen adsorption on polyethylene. For this type of isotherm, adsorption continuously increase with increase in relative pressure and adsorbate-adsorbate interactions play a significant part [50].

Type-IV is for mesoporous solids. Its significant feature is the hysteresis loop, that is linked with capillary condensation that takes place is mesopores. The overall shape is almost the same as type-II, and the difference is in different routes for adsorption and desorption. The right-side path is for adsorption, and the left-side for desorption [50].

Type-V is also uncommon and is comparative to type-III. This observable for only some of the porous adsorbents when adsorbent-adsorbate interactions are weak [50].

Type-VI indicates multilayer adsorption on non-porous surface of uniform nature. It is because of this multilayer adsorption that the steps are observed. Each step height represents the capacity

of single layer. The step size and gradient depend on the temperature and overall system. One example is of argon adsorption on carbon black [50].

Actual isotherms are combinations of these IUPAC types and previous knowledge of material helps understand these curves better.

3.2.2 Langmuir isotherm

The Langmuir isotherm is one of the simplest models available to represent the absorbent and adsorbate interactions. IUPAC type-I shape is often given by the Langmuir isotherm. There are several assumptions that are made in defining the Langmuir isotherm. These assumptions given by Hammond et al. [52] and Sahu et al. [53] are as follows:

- Only a single adsorbate molecule can attach with one active site of the adsorbent. This means its valid for monolayer adsorption.
- All the active sites are identical.
- Inter-particle interactions are neglected, meaning that adsorbate and adsorbent interactions are independent of the neighboring molecules.
- The heat of adsorption is the same as the activation energy required for desorption.
- Ideal gas law is followed in the vapor phase.

The Langmuir equation (Eq.3.1) [52] is given as:

$$q = \frac{q_s b\, p_i}{1 + b\, p_i} \tag{3.1}$$

Here,

q is the adsorption capacity, kmol kg $^{-1}$

p_i is the partial pressure of component i, bar

q_s is the maximum adsorption capacity, kmol kg $^{-1}$

b is the Langmuir parameter, bar $^{-1}$

Different variations and extended versions of Langmuir isotherm are used to make it useful depending on the situation. For example, Extended Langmuir is often applied for multicomponent systems. The Langmuir variations used in Aspen Adsorption® are given in Table 3. Eq. 3.1 is given as Langmuir 1 in Aspen Adsorption®. The fitting parameters are changed with IP notation. Loading in software is given with a w_i, but for simplicity it is given with q everywhere. More details of these equations can be found in software's help [54].

Table 3. Langmuir isotherm variations

Isotherm names	**Isotherm equations**
Langmuir 1	$q = \frac{IP_1 p_i}{1 + IP_2 p_i}$ (3.2)
Langmuir 2	$q = \frac{IP_1 exp^{\frac{IP_2}{T_s}} P_i}{1 + IP_3 exp^{\frac{IP_4}{T_s}} P_i}$ (3.3)
Langmuir 3	$q = \frac{(IP_1 - IP_2 T_s) IP_3 exp^{\frac{IP_4}{T_s}} p_i}{1 + IP_3 exp^{\frac{IP_4}{T_s}} p_i}$ (3.4)
Extended Langmuir 1	$q = \frac{IP_{1i} p_i}{1 + \sum_k (IP_{2k} p_k)}$ (3.5)
Extended Langmuir 2	$q = \frac{IP_{1i} exp^{\frac{IP_{2i}}{T_s}} P_i}{1 + \sum_k (IP_{3k} exp^{\frac{IP_{4k}}{T_s}} P_k)}$ (3.6)
Extended Langmuir 3	$q = \frac{(IP_{1i} - IP_{2i} T_s) IP_{3i} exp^{\frac{IP_{4i}}{T_s}} p_i}{1 + \sum_k (IP_{3k} exp^{\frac{IP_4}{T_s}} p_k)}$ (3.7)

Langmuir 1 and extended Langmuir 1 are only functions of partial pressure, whereas, Langmuir 2 and its extended form is also dependent on the temperature, making them more accurate. Here T_s is the saturation temperature. Langmuir 3 and extended Langmuir 3 is a function of temperature and partial pressure, but additionally the maximum loading is also given as a function of temperature, making it the most accurate option.

Simple Langmuir isotherms can be used for single component systems, and extended versions for the multicomponent systems.

3.2.3 Freundlich isotherm

This is one of the simplest non-linear empirical equation. Heterogeneous adsorption surface is assumed for this isotherm equation, and it is also assumed that with increase in concentration the adsorbed amount is infinitely increased [55]. Following is the equation (Eq. 3.8) that is applicable for gas phase:

$$q = k_F p_i^{\frac{1}{n_F}} \quad (3.8)$$

Here,

q is the adsorption capacity, kmol kg $^{-1}$

k_F is the Freundlich constant, kmol kg^{-1} bar^{-1}

p_i is the partial pressure of component i, bar

n_F is the heterogeneity factor

In Aspen Adsorption® these models are given as Freundlich 1 and Freundlich 2. They are given in equations 3.9 and 3.10, respectively.

$$q = IP_1 P_i^{IP_2} \tag{3.9}$$

$$q = IP_1 exp^{\frac{IP_3}{T_s}} p_i^{IP_2} \tag{3.10}$$

Freundlich 1 is only a function of partial pressure, and Freundlich 2 that is a function of partial pressure and temperature is a more accurate option to use, but simulation will take longer to run.

3.2.4 The Brunauer-Emmett-Teller (BET) isotherm

BET isotherm is an extended form of Langmuir, and it is based on model for multilayer adsorption [56]. It assumes that molecules behave in such a way that they are in bulk liquid, that molecules are not only adsorbed on adsorbing sites but also on the other adsorbed molecules, number of adsorbing sites per layer are constant, and that the adsorbing sites first-layer energy is identical.

The basic BET equation (Eq. 3.11) is as follows:

$$\frac{\frac{p_i}{p_{sat}}}{q(1-\frac{p_i}{p_{sat}})} = \frac{1}{q_m c} + \frac{c-1}{q_m c}\left(\frac{p_i}{p_{sat}}\right) \tag{3.11}$$

Here,

$\frac{p_i}{p_{sat}}$ is the relative pressure

q_m is the BET monolayer capacity, kmol kg^{-1}

c is the parameter related to heat of adsorption

In Aspen Adsorption® one variation of BET isotherm is given as:

$$q = \frac{IP_1 p_i exp\left(\frac{IP_2}{T_s}\right)}{\left[1 + IP_3 p_i exp\left(\frac{IP_4}{T_s}\right)\right]\left[1 - IP_5 p_i exp\left(\frac{IP_6}{T_s}\right)\right]} \quad (3.12)$$

3.2.5 Toth isotherm

Toth isotherm is an empirical isotherm that is used in gas-phase adsorption. It is one of the variations of the Langmuir isotherm. It correlates the absolute amount adsorbed at a given temperature and pressure [57]. This is most suitable for heterogeneous adsorption sites, and has a lower error compared with the Langmuir isotherm [46]. Toth isotherm equation is presented below:

$$q = \frac{q_0 b_T p_i}{(1 + (bp_i)^j)^{\frac{1}{j}}} \quad (3.13)$$

Here,

q_0 is the amount adsorbed at saturation, kmol kg $^{-1}$

j is the heterogeneity parameter, kmol kg $^{-1}$

b_T is the adsorption affinity, bar $^{-1}$. Further given as following:

$$b_T = b_0 \, exp \, exp\left(\frac{\Delta H}{RT}\right) \quad (3.14)$$

and here,

b_0 is the adsorption affinity at infinite temperature, bar $^{-1}$

ΔH is the heat of adsorption, kJ mol $^{-1}$

R is the universal gas constant, kJ mol $^{-1}$ K^{-1}

T is the temperature, K

In Aspen Adsorption® Toth isotherm is given as:

$$q = \left[\frac{(IP_1 p_i)^{IP_2}}{1 + (IP_3 p_i)^{IP_2}}\right]^{\frac{1}{IP_2}} \tag{3.15}$$

3.2.6 Experimental data for adsorption isotherms

In this chapter we look at some of the experimental data found in literature for CO_2 and H_2O adsorption isotherms. Moreover. we look at how well this experimental data fit with certain isotherm models.

Figure 7 [58] shows the plot of H_2O adsorption on 3A crystals. Data points are from the experimental data and the solid lines shows the model fitting through triple-site Langmuir model. This type of model fits very well with the experimental data.

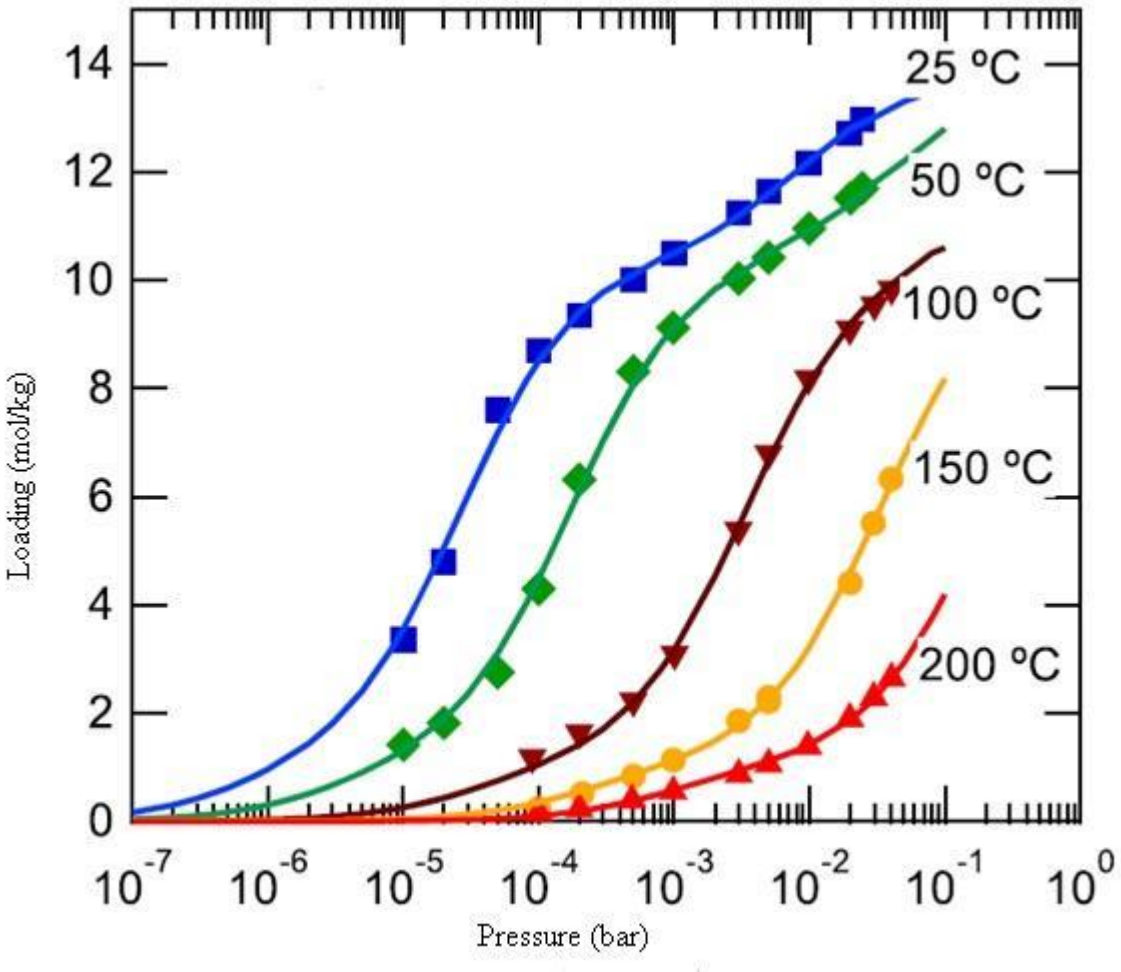

Figure 7. H_2O isotherm of 3A crystals at different temperatures. Model is fitted using triple-site Langmuir model

The tabulated data for Figure 7 is given in appendix-I and data is available for 4A crystals in the same appendix.

Isotherms in Figure 7 follow the type-II of IUPAC classification, that is usually for multilayer adsorption. Model used is triple-site Langmuir given in Eq. 3.16:

$$q = \frac{q_{s1} b_1 p_i}{1 + b_1 p_i} + \frac{q_{s2} b_2 p_i}{1 + b_2 p_i} + \frac{q_{s3} b_3 p_i}{1 + b_3 p_i} \tag{3.16}$$

Here,

q is the adsorption capacity, kmol kg $^{-1}$

p_i is the partial pressure, bar

q_s is the maximum adsorption capacity, kmol kg $^{-1}$

b is the affinity parameter, bar $^{-1}$

Further, $b_1$is given as:

$$b_1 = b_{10} exp\left(\frac{\Delta H_1}{RT}\right) \tag{3.17}$$

The number in subscript of b represents the sites, and similar equation is used for $b_2$and b_3.

Fitting parameters are given in Table 4.

Table 4. Fitting parameters for triple-site Langmuir for H_2O on 3A crystals.

Parameters				
q_{s1}**(mol/kg)**	b_{10} **(1/bar)**	ΔH_1**(kJ/mol)**	q_{s2}**(mol/kg)**	b_{20} **(1/bar)**
9.37	1.26×10^{-6}	59.75	1.06	4.67×10^{-3}
Parameters				
ΔH_2**(kJ/mol)**	q_{s3}**(mol/kg)**	b_{30} **(1/bar)**	ΔH_3**(kJ/mol)**	
48.37	3.35	1.15	51.42	

Experimental data for H_2O isotherm on molecular sieve 3A has been given by Lin et al. [59] Tables 5 and 6 represents this data for different temperatures.

Table 5. Experimental data for H20 at 25 and 40 °C for molecular sieve 3A

T = 25 °C		**T = 40 °C**	
p (kPa)	q(mol/kg)	p (kPa)	q(mol/kg)
3.11×10^{-4}	1.54	4.66×10^{-4}	1.50
5.53×10^{-4}	2.78	9.91×10^{-4}	2.06
1.06×10^{-3}	5.83	2.59×10^{-3}	3.61

Continuation of Table 5.

3.96×10^{-3}	8.00	5.38×10^{-3}	5.50
1.31×10^{-2}	8.69	9.48×10^{-3}	6.81
3.82×10^{-2}	9.25	2.06×10^{-2}	7.72
9.79×10^{-2}	9.72	3.63×10^{-2}	8..36
3.97×10^{-1}	10.67	7.83×10^{-2}	8.64
8.82×10^{-1}	10.89	1.66×10^{-1}	9.17
1.24	11.33	6.09×10^{-1}	10.00
		1.225	10.00

Table 6. Experimental data for H20 at 60 and 80 °C for molecular sieve 3A

T = 60 °C		**T = 80 °C**	
p (kPa)	q(mol/kg)	p (kPa)	q(mol/kg)
1.15×10^{-3}	1.11	3.42×10^{-3}	1.04
2.94×10^{-3}	1.71	1.32×10^{-2}	1.97
8.06×10^{-3}	2.78	4.55×10^{-2}	4.06
1.37×10^{-2}	4.68	8.14×10^{-2}	5.86
3.07×10^{-2}	6.34	1.43×10^{-1}	6.44
6.30×10^{-2}	7.69	8.82×10^{-1}	8.31
1.35×10^{-1}	8.39	1.95	8.61
3.73×10^{-1}	9.09		
7.61×10^{-1}	9.32		
1.17	10.06		

For a molecular sieve kind adsorbent zeolite 13-X Figure 8 [60] shows the isotherms with Langmuir-Freundlich isotherm model. This data is gathered for a TSA process. Tabulated experimental data can be found in Appendix-I.

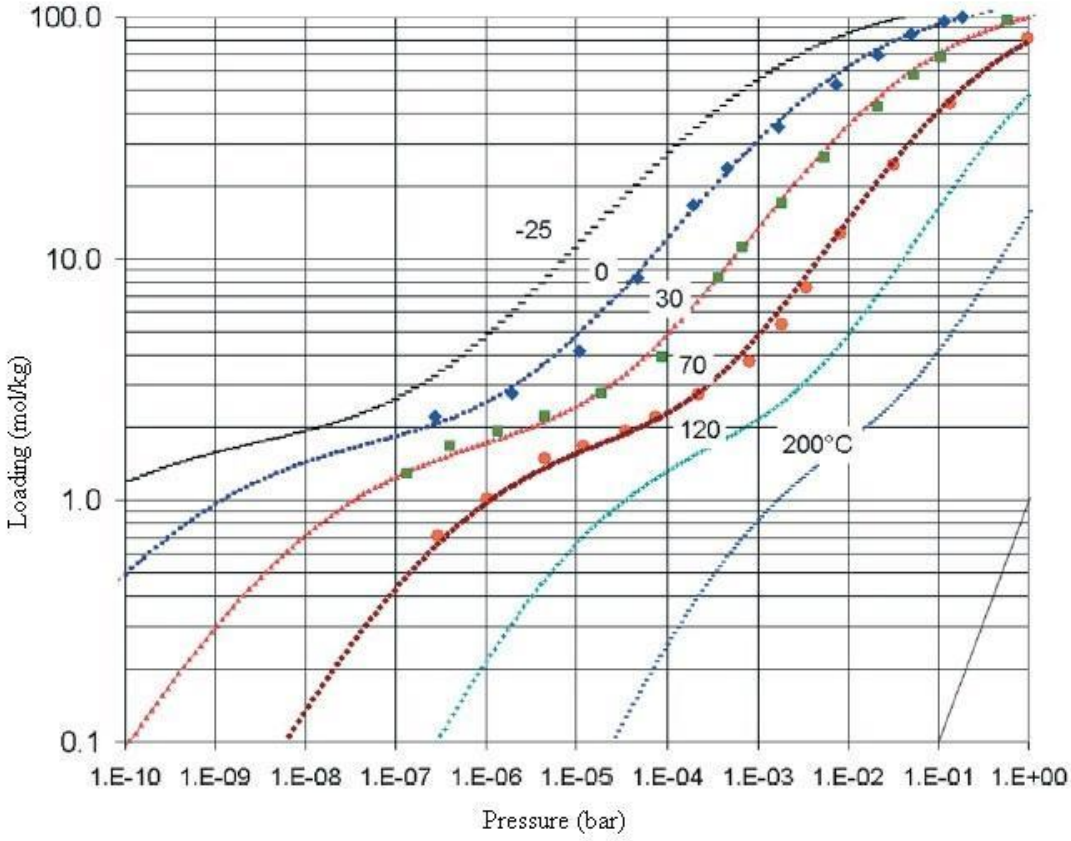

Figure 8. CO_2 isotherm of 13-X molecular sieves at different temperatures

3.3 Adsorption processes

Gases are attracted differently to the solid adsorbents, some bond more strongly than the others. This difference helps in the separation of different species of gasses [61]. The process to separate the gas is carried out in cycles of adsorption and desorption. This is made possible with the swing adsorption techniques. These techniques consist of Pressure Swing Adsorption (PSA), Vacuum Pressure Swing Adsorption (VPSA), Temperature Swing Adsorption (TSA), and Electric Swing Adsorption (ESA). Moreover, these methods can be used in a hybrid setup [62].

3.3.1 Pressure Swing Adsorption

In this technique high pressure is used to absorb the gas, and then pressure is reduced to regenerate the adsorbent [63]. It is important to note here that pressure always stays above the atmospheric pressure [64]. We can say that driving force is the pressure difference between adsorption and desorption steps. This technique has been used for processes where feed streams are at high pressure and low temperatures. The examples of such industrial processes include production of H_2 and purification of natural gas [65]. The actual pressure, the adsorbent material,

and the process cycle configuration all depends on the species involved in the feed stream. For instance, in CO_2 separation, it depends on whether capturing is done before or after combustion. For post-combustion separation, VSA is more common, and it is discussed in next section.

The benchmark process for this technique is called a Skarstrom cycle. This cycle is based on two parallel packed beds and involves four different steps for complete adsorption and then desorption [66]. The purpose of two beds is that when one bed is being fed for adsorption, the other bed is being regenerated and prepared for the adsorption cycle.

In the Skarstrom cycle, first step is the pressurization with feed, then the heavy component is adsorbed, in the third step is to reduce the pressure, and in the final step adsorbed component is completely withdrawn [65]. The technical terms for these steps are pressurization, feed adsorption, blowdown and then purge [66]. Several other variations are available in case of CO_2 separation to increase the purity and recovery, and to reduce the overall cost. One such step is pressure equalization between the two beds, this especially helps with lowering the costs related to the compressors. Nonetheless, these steps are also dependent on the material used for the adsorbent.

One example where PSA is being applied successfully is the air separation. N_2 and O_2 are recovered as different streams as the result, and the specie being adsorbed depends on the type of adsorbent used. Two PSA units can be used in series for instance, to get high purity oxygen. A patented method by Hayashi et al. [67] first use an adsorption column with zeolite as adsorbent to capture N_2, and then another column in series with carbon molecular sieve to retrieve pure argon.

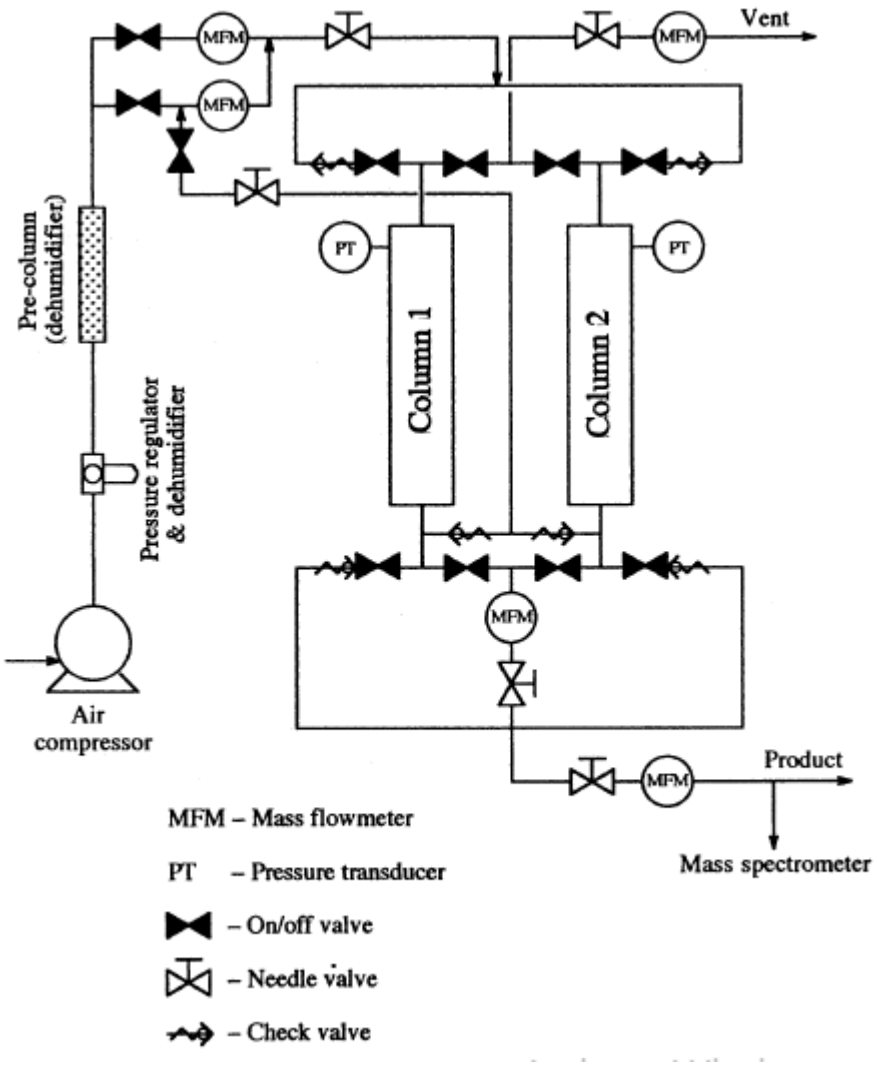

Figure 9. PSA experimental setup [68]

Figure 9 shows a setup for air separation that is made for PSA adsorption and operates on the previously mentioned Skarstrom cycle.

3.3.2 Vacuum Pressure Swing Adsorption

VSA is used for process conditions where pressure of flue gases is near atmospheric pressure. Therefore, the material used as adsorbent should have a much higher attraction for the key component. This allows the adsorption to take place near atmospheric pressure, without the need of compressing the feed stream. On the other hand, vacuum is required for the regeneration step, that requires vacuum pumps [63].

Like PSA, the Skarstrom cycle is used as the benchmark. As mentioned before, this method is suitable for the post-combustion separation.

3.3.3 Temperature Swing Adsorption

When the change in the pressure is not a strong enough driving force for the strongly adsorbed components, TSA is a preferred choice [69]. In TSA, adsorption step is carried out a low temperature, and desorption at a higher temperature. This high temperature is applied at near atmospheric pressure. Lower temperature increases the uptake of gas being adsorbed because adsorption is an exothermic process [64]. Again, the modified forms of Skarstrom cycle are utilized for TSA.

This method is useful where waste heat can be readily found, and that heat can further be utilized for adsorbent regeneration. This takes away the need of compressors or vacuum pumps required for PSA or VSA [62]. Such a situation is present in coal-powered power plants for the post-combustion capture of carbon dioxide [70].

3.3.4 Electric Swing Adsorption

This method is based on the TSA, but instead of using heat directly through means of a diluent, electric current is used to generate the heat. The heat is generated by passing the current directly through a conducting material, phenomenon known as the Joule effect [71], [72]. For ESA specifically, current is passed through the adsorbent material, and for this matter adsorbent for ESA must be a conducting material. This is achieved by mixing the conducting material such as graphite with the adsorbent material [72].

3.4 Modelling of adsorption processes

Mathematical modelling of adsorption process is necessary to evaluate adsorption kinetics, to size adsorbers and to design and optimize adsorption processes.

Mathematical modelling in Aspen Adsorption is based on several different equations. There are multiple options available to choose from. For example, only for momentum balance calculations, one can choose between Burke-Plummer equation, Darcy's law, Ergun equation, Karman-Kozeny equation, and simple constant pressure options. Some of the common options used for the modelling of fixed bed adsorber are discussed here. Modelling equations are included for material and momentum balance, kinetics, and energy balance. Isotherms are already studied in chapter 3.2.

Several models have been proposed to study the kinetics of the adsorption processes. These models include Kopelman, Ho and Mckay, Brouers and Stolonogo-Costain, and the model proposed by Haerifar, Azizian, Bashiri and Shajari. Most widely used model to study kinetics is given by Lagergren [73].

Component mass balance:

This component balance equation is based on the continuity equation that is obtained by applying the law of conservation of mass to a differential control volume. The control volume in this case in one direction, that is z. The component balance equation is given in Eq. 3.18 by Seidel [74].

$$-\frac{\partial}{\partial z}\left(D_{ax}\frac{\partial C_i}{\partial z}\right)+\frac{\partial(vC_i)}{\partial z}+\frac{\partial C_i}{\partial t}+\frac{(1-\varepsilon)}{\varepsilon}\frac{\partial \bar{q}_i}{\partial t}=0 i=1,\dots,n \qquad (3.18)$$

Here,

D_{ax} is the axial dispersion coefficient, $m^2 s^{-1}$

v is the interstitial fluid velocity, $m\ s^{-1}$

C is the concentration, $mol\ m^{-3}$

z is the length along z direction, m

t is time, s

ε is the bed void fraction

$\bar{q}_i$ is the average solid loading, $mol\ kg^{-1}$

The first term in Eq. 3.18 $-\frac{\partial}{\partial z}\left(D_{ax}\frac{\partial C_i}{\partial z}\right)$ represents the axial dispersion [75]. The second factor in $\frac{\partial(vC_i)}{\partial z}$ represents the velocity dependent material balance in direction z. The third factor $\frac{\partial C_i}{\partial t}$ is for the change in concentration with respect to time. The last factor $\frac{(1-\varepsilon)}{\varepsilon}\frac{\partial \bar{q}_i}{\partial t}$ is for the loading or accumulation in the porous part of the solid adsorbent.

The value of the axial dispersion coefficient can be obtained experimentally. This is done by injecting the tracer pulse in the column and recording the concentration changes [76].

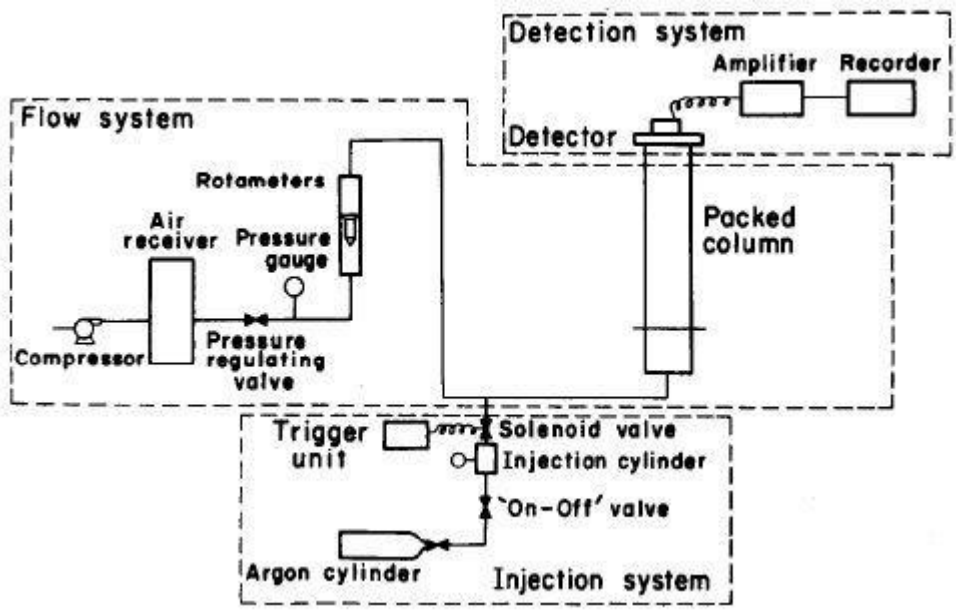

Figure 10. Dispersion coefficient determining apparatus [76].

Figure 10 shows the common apparatus used for getting the values of axial dispersion coefficient. Air is continuously passed through the packed bed column, and argon is pulsed through the same stream of air to the packed column. These pulses are detected at the other end and the concentration profiles are plotted to determine the dispersion coefficients. After performing these experiments, the dispersion coefficient can be correlated with Eq. 3.19 [76].

$$D_{ax} = \frac{0.25 D_M}{\varepsilon} + \frac{0.28 D_M}{\varepsilon}\left(\frac{\varepsilon v d_p}{D_M}\right)^{1.4} \tag{3.19}$$

Here,

D_M is molecular diffusivity, $m^2\ s^{-1}$

ε is the bed void fraction

v is the interstitial velocity, $m\ s^{-1}$

$d_p$is the diameter of the particle, m

Note: Eq. 3.19 is valid only for ($0.2 < Re < 4$).

Alternatively, dispersion coefficient can be correlated by the equation (Eq.3.20) given by Edwards et al [76].

$$D_{ax} = 0.73 D_M + \frac{0.5\, v d_p}{1 + (9.7 D_M)/(v d_p)} \tag{3.20}$$

Eq. 3.20 is true for (0.08 < Re < 50) and (0.0377 < d_p< 0.60 cm)

Here,

D_M is molecular diffusivity, m^2 s^{-1}

v is the interstitial velocity, m s^{-1}

$d_p$is the diameter of the particle, m

Total mass balance:

$$\frac{\partial(vC)}{\partial z}+\frac{\partial C}{\partial t}+\frac{(1-\varepsilon)}{\varepsilon}\sum_{i=1}^{n}\frac{\partial \bar{q}_i}{\partial t}=0 \tag{3.21}$$

Total mass balance is applied to the complete system with inlet and outlet as the boundaries. This simplifies the component mass balance and takes away the need of diffusion term.

Ideal gas law:

$$C=\frac{p}{RT} \tag{3.22}$$

Energy balance:

The energy balance equation in Eq.3.23 is given by Anna et al. [77]. This equation is used for energy balance calculations in the simulation.

$$-\frac{K_{ax}}{\varepsilon}\frac{\partial^2 T}{\partial z^2}+\frac{C_{p,g}}{R}\frac{\partial(vp)}{\partial z}-\frac{C_{p,g}}{R}\frac{\partial p}{\partial t}+\left[\frac{1-\varepsilon}{\varepsilon}\left(\rho C_{p,s}+C_{p,a}\sum_{i=1}^{n}\bar{q}_i\right)\right]\frac{\partial T}{\partial t}+\frac{1-\varepsilon}{\varepsilon}C_{p,a}T\sum_{i=1}^{n}\frac{\partial \bar{q}_i}{\partial t}$$
$$+\frac{1+\varepsilon}{\varepsilon}\sum_{i=1}^{n}\left((-\Delta H_i)\frac{\partial \bar{q}_i}{\partial t}\right)-\frac{2h_{in}}{\varepsilon r_{in}}(T-T_w)=0 \tag{3.23}$$

Here,

K_{ax} is the thermal conductivity, W m^{-1} K^{-1}

$C_{p,g}$ is the heat capacity, J K^{-1}

h_{in} is the heat transfer coefficient, W m^{-2} K^{-1}

r_{in} is the internal radius, m

T_w is the temperature of the wall, K

Linear Driving Force (LDF) model:

The LDF model for mass transfer was initially given in 1947 by Gleuckauf and Coates [59], [78]. The model is analytically simple and can be easily applied. It is assumed for the model that there is no radial change in temperature for the adsorbate. The model equation is given in Eq. 3.24.

$$\frac{\partial q}{\partial t} = k_{LDF}(q_e - \bar{\mathrm{q}}) \tag{3.24}$$

Here,

$\bar{\mathrm{q}}$ is the average transient adsorbent loading, kmol kg $^{-1}$

q_e is the equilibrium adsorbent loading, kmol kg^{-1}

t is time, s

k_{LDF} is the LDF mass transfer coefficient, s $^{-1}$. Eq. 3.25 [59] shows how it can be determined experimentally.

$$k_{LDF} = -\frac{ln\left\{\frac{q_e - \bar{\mathrm{q}}}{q_e}\right\}}{t} \tag{3.25}$$

In Aspen Adsorption® the LDF model is given as the "Linear Lumped Resistance" model, which is the same as Eq. 3.24 for the solid loading. The notation used for the k_{LDF} is the mass transfer coefficient (MTC).

The equation that is generally used to calculate pressure drop in the packed bed is the Ergun equation (Eq. 3.25) [49], that is a combination of Carman-Kozeny (Eq. 3.26) [49] and Burke-Plummer equations (Eq. 3.27) [49]. Carman-Kozeny equation is valid only for the laminar flow. Whereas Burke-Plummer equation is used when the flow is turbulent. Since Ergun equation is a combination of both these equations, it is applicable to both the laminar and turbulent flows.

Ergun equation:

$$\frac{\partial p}{\partial z} = -\left(1.5 \times 10^{-3}\frac{\mu(1-\varepsilon_i)^2}{\left(2r_p\psi\right)^2\varepsilon_i^3}v_g + 1.75 \times 10^{-3}\frac{\rho_g M_r(1-\varepsilon_i)}{2r_p\psi\varepsilon_i^3}v_g^2\right) \tag{3.26}$$

Carman-Kozeny equation:

$$\frac{\partial p}{\partial z} = -1.5 \times 10^{-3} \frac{\mu(1-\varepsilon_i)^2}{\left(2r_p\psi\right)^2 \varepsilon_i^3} v_g \tag{3.27}$$

Burke-Plummer equation:

$$\frac{\partial p}{\partial z} = -1.75 \times 10^{-3} \frac{\rho_g M_r (1-\varepsilon_i)}{2r_p \psi \varepsilon_i^3} v_g^2 \tag{3.28}$$

Here,

p is pressure, Pa

z is the direction along which pressure drops, m

μ is gas viscosity, Pa s

ε_i is bed void fraction or porosity

$(1-\varepsilon_i)$ the solid part

r_p is radius of the particle, m

ψ is a shape factor

$v_g$is velocity of gas

ρ_g is density of gas, kg/m^3

M_r is molecular weight, kg/kmol

3.5 Industrial applications and involved industries

Adsorption has gradually found applications in several industrial processes. Some of the earliest and most established applications are related to the purification and separation of different gas streams including air. It further includes purification of water, recovery of essential chemicals from waste streams, and drying of liquids and gases [79].

The separation of *n*-paraffins from the iso-paraffin and cyclic hydrocarbons is carried out using the Sorbex^{TM} technique of adsorption. Sorbex^{TM} is a commercial process that is applied by the UOP-Honeywell group of companies. This company provides one of the largest range of adsorbents and adsorption equipment Sorbex^{TM} process was commercialized in the 1960s and

since then other variations of the process have been commercialized as well. This process basically simulates a moving bed without using an actual moving bed. This involves a special configuration with multi-bed stationary adsorbent chambers, with counter-current extraction [80]. The MX Sorbex™ process was commercialized in 1998 and is used to produce highly pure meta-xylene. Similarly, for the separation of para-xylene UOP Parex™ adsorption process is utilized to obtain pure para-xylene form the mixture of C_8 aromatics isomers. Initially commercialized in 1971, this process now uses ADS-47 adsorbent that not only offers a high capacity, but lowest pressure drop as well.

Figure 11 shows the MX Sorbex™ that shows how adsorption is integrated in the complete process.

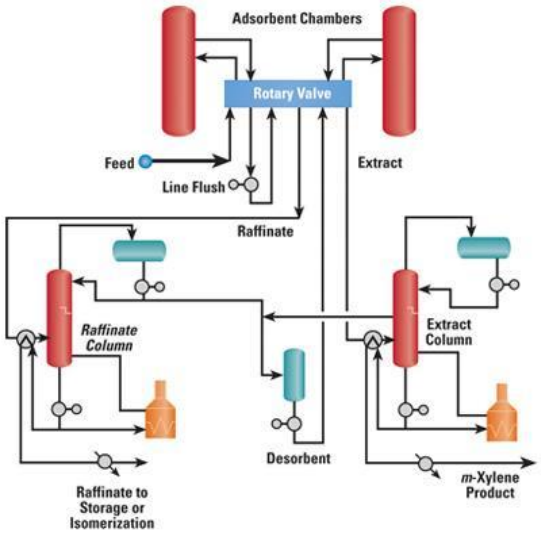

Figure 11. UOP- MX Sorbex Process

Apart from this, UOP-Honeywell provides adsorbents for numerous applications including air separation, medical grade oxygen, nuclear waste, petrochemicals, refining, and natural gas. For instance, adsorbents available for air separation offer sulfur removal for carbon dioxide, moisture removal, and suitable adsorbents for both PSA and VSA systems.

Adsorption is also used for the separation of CO_2 from the natural gas, drying of solvents, natural gas and liquid paraffins. UOP also provides services for natural gas processing.

Conventionally, cryogenic processes are used for the separation of nitrogen from air, but with the development of PSA technology, adsorption can be used commercially. This mechanism utilizes the difference between transport rates of different molecules. With the change of adsorbent type, product can be freely selected between nitrogen or oxygen. Zeolite-based adsorbents preferentially absorb nitrogen, while carbon molecular sieves can be applied to absorb oxygen and let through the nitrogen.

Solvent recovery is another application where adsorption can be used successfully. Industries where solvent recovery is required include adhesives, explosives, rayons, paints, polymers, and

oil extraction from seeds. Durr-megtec is one of the companies that provide more than 99 percent recovery of the solvents using a carbon adsorption technology [81]. This method works by removing the volatile organic compounds (VOCs) on to the activated carbon adsorber. Other prominent companies for solvent recovery include Jacobi group, and Ventilzaione Industraile Srl.

4 ASPEN ADSORPTION

Aspen Adsorption® is a software developed by Aspen Tech for the specific purpose of simulating adsorption processes. Apart from flowsheet simulations, this software can be used for optimum design and optimization. The basic aim of using this software is the selection of suitable adsorbents, to size the units and adsorption columns properly, and to design more efficient adsorption cycles. A comprehensive chapter about the simulations of adsorption processes using Aspen Adsorption® is written in a book by Wood et al [49]: "Design, Simulation, and Optimization of Adsorptive and Chromatographic Separations: A Hands-on Approach". This book was used to get the basic idea of the software and to set-up the initial few simulations.

This software is deemed suitable for the simulation of liquid adsorption processes, gas cyclic steady state models, gas dynamic adsorption models, ion exchange, and reactive gas adsorption processes.

Within the software there are several templates and demonstrations available that can be used to make your own comprehensive models. Some examples of such demonstrations include simple breakthrough runs for air separation, TSA, VSA, and PSA models for several components, and a case involving reactive adsorption. In the next section we look at the basic components of Aspen Adsorption and how to completely define the adsorption bed called Gas_Bed in this software.

4.1 Aspen Adsorption interface

Figure 12 shows the initial interface of the software. The run mode, currently at dynamic can be changed to four other settings. These settings include initialization, steady state, estimation, and optimization.

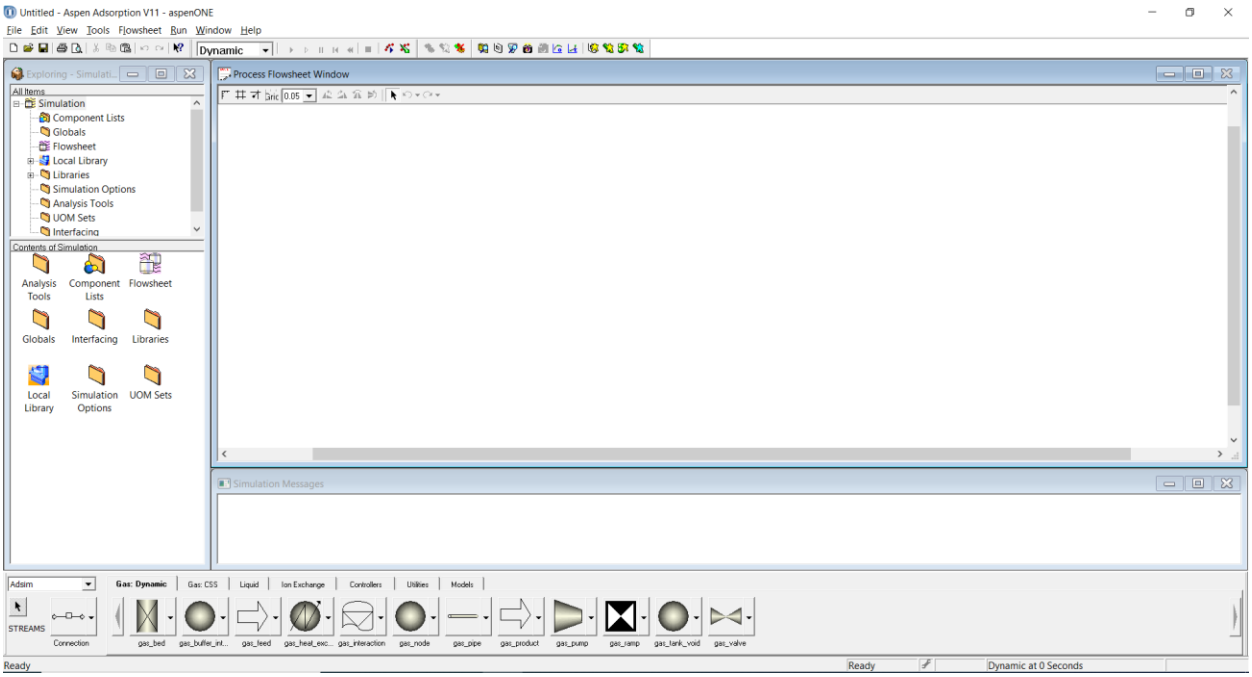

Figure 12. Initial interface for Aspen Adsorption

4.2 Selection of components

The first thing that is required in Aspen adsorption is to define the component list. The best way is to import these components from Aspen Properties, where both the components and suitable physical property methods can be selected. The following steps are general guidelines for adding the components:

i. Under the **"All Items"** window of **"Exploring-Simulation"** tab of the main interface, click on the **"Component Lists"** folder.

ii. Under the second window of **"Exploring-Simulation"** tab, that would now say **"Contents of Component Lists"**, three options would be available. Double-click on **"Configure Properties"**. A window would open as shown in Figure 13.

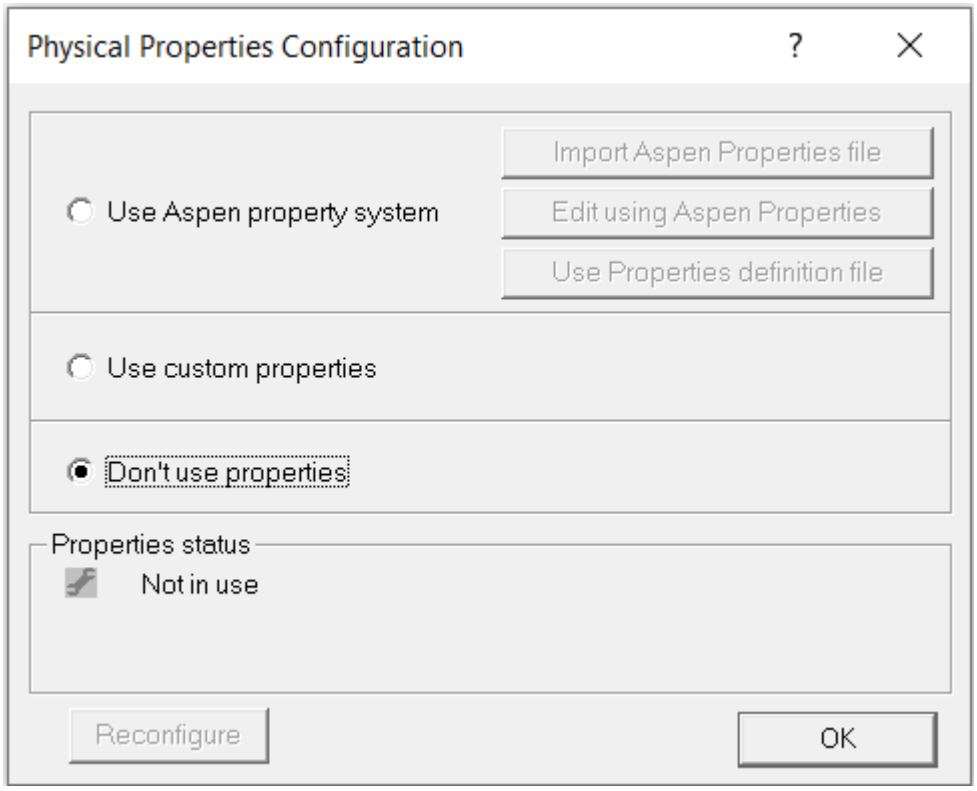

Figure 13. Physical properties window for the selection of components

iii. Check the **"Use Aspen property system"** option. Then click on **"Edit using Aspen properties"**, that is the second option in the window.

iv. Aspen Plus would open for the selection of components and properties method. The window is shown in Figure 14. For this example, Water and Nitrogen are shown. Then click on **"Methods"** tab and choose a suitable property method. For these components, **UNIQUAC** works fine.

v. Click on the **"Run"** button and then go back to Aspen Adsorption window. Click on OK. Then go back to Aspen Properties and click on yes option for saving a backup file.

vi. Now a "Build Component List" window would open, transfer to components to right-hand side, under the components tab and click OK. This is shown in Figure 15.

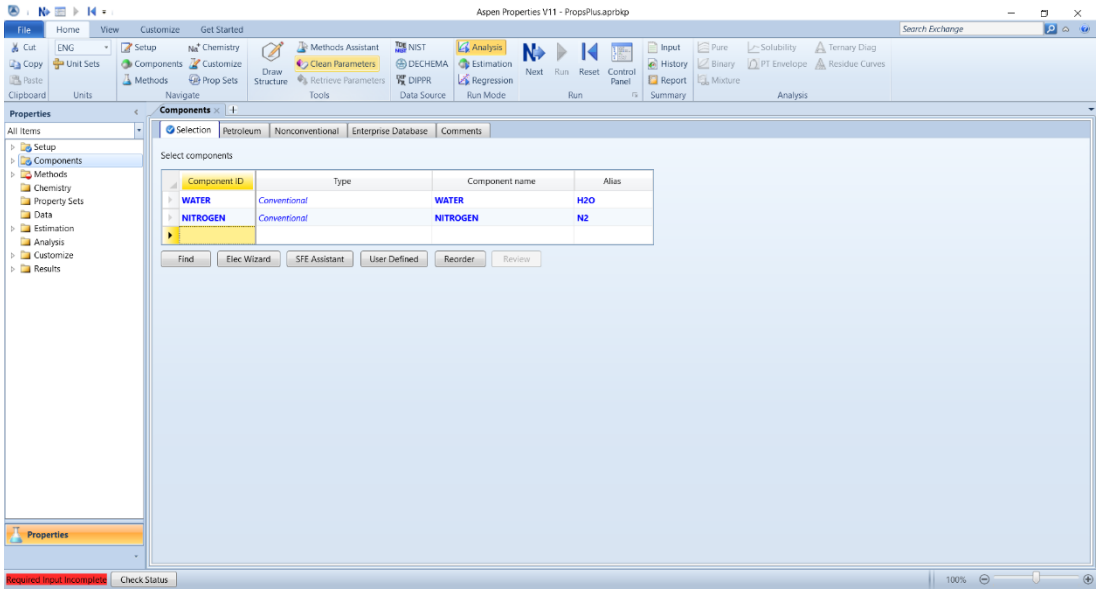

Figure 14. Selection of components and methods with the help of Aspen properties

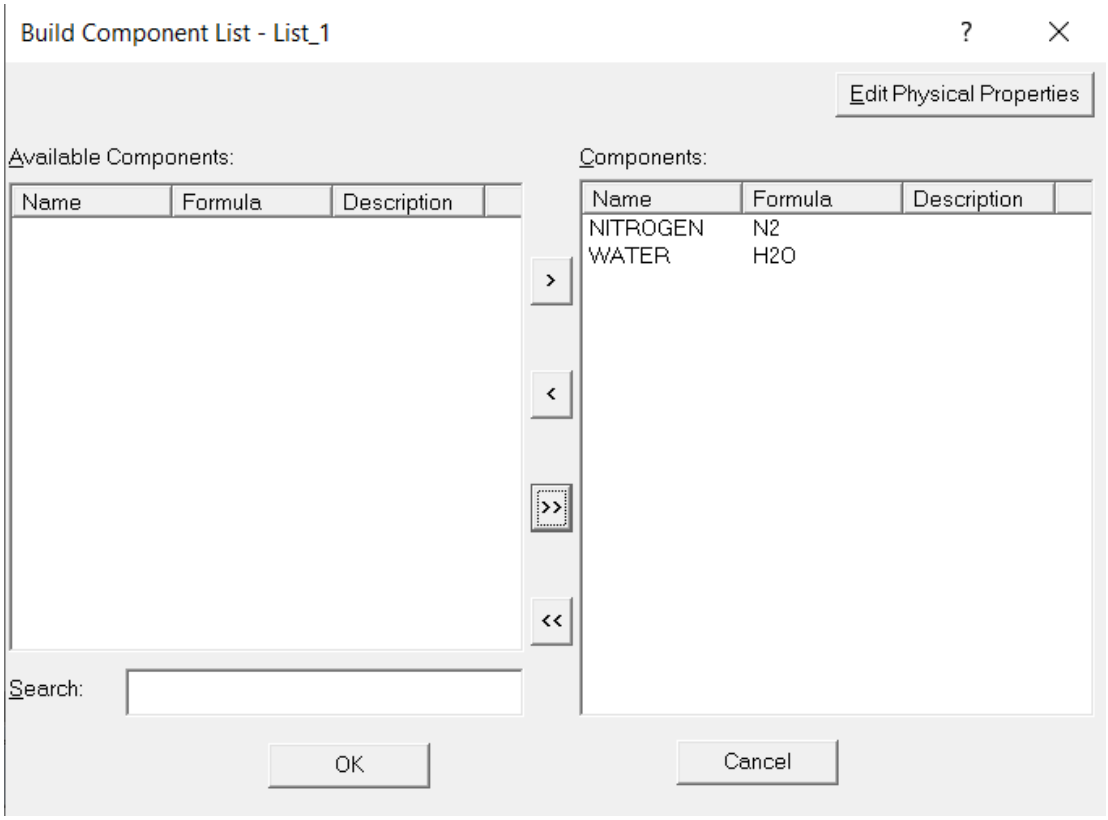

Figure 15. Build component list window

4.3 Configuration of the Adsorbent Bed

The scope of the thesis is dynamic adsorption of different gases on solids. The models and options available are shown in Figure 16.

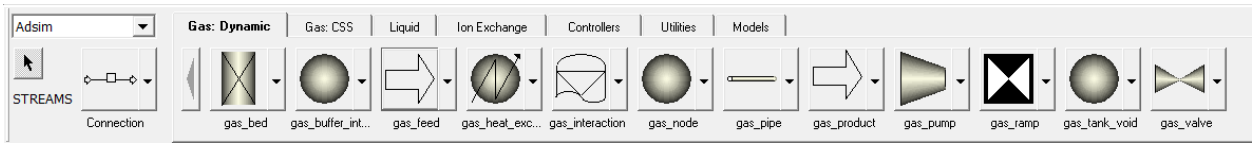

Figure 16. Available model options under Gas: Dynamic window

The main component that is extensively defined is the gas_bed for adsorption. The following steps can be followed to define the gas_bed:

i. Click on the **gas_bed** icon once and left-click anywhere on the main flowsheet once. Then right-click anywhere to stop placing more gas_beds. Double-click on the gas_bed that is now on the main flowsheet.

ii. Block configuration would open as shown in Figure 17. The default options are the simplest with only one layer within the vertical bed, without any internal heat exchanger.

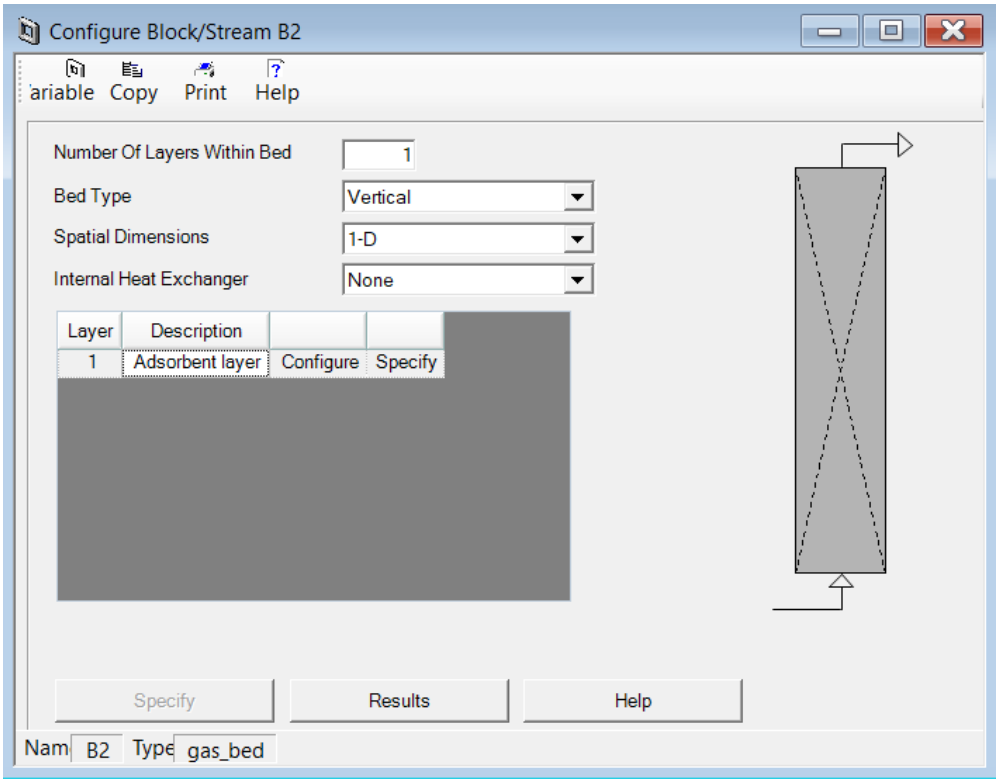

Figure 17. Configuration window for the adsorption column

iii. Click on the **"Configure"** option. There are seven different tabs, and the **"General"** tab is what opens first, shown in Figure 18. The upwind differencing scheme 1 (UDS1) is the default option for Discretization of partial differential equations (PDEs) and is suitable for most cases. Discretization is a method by which complex PDEs are converted to system of coupled ordinary differential equations (ODEs) [82]. Solution

of these equations gives an approximate result but makes the processing by computers relatively easier and faster.
For USD1 scheme, the results are quite accurate and computation time is fast for the dynamic models [49]. This is scheme is based on the first-order Taylor expansion, and is stable for the first-order equations. Other available methods are upwind differencing scheme 2 (UDS2), central differencing scheme 1 and 2 (CDS1 and CDS2), biased upwind differencing scheme (BUDS), Flux limiter, Fromm's scheme, quadratic upwind scheme (QDS), Leonard differencing scheme (LDS), and mixed differencing scheme [54]. The detailed equations for these schemes are given in Aspen's help [54].

UDS2 can be used for a second-order accuracy, but is known to generate oscillations in the system. If axial dispersion is included in the bed settings, then it is a good option to use CDS1 or CDS2. Numerical instabilities should be considered when using these options. BUDS can be applied for extremely non-linear problems. Lower number of nodes should be chosen for reasonable simulation time as accuracy is covered with the fourth-order accuracy of the scheme. Flux limiter has the accuracy of higher order differencing schemes but the stability of UDS1. Fromm's scheme is the combination of first and second order schemes and may produce large number of instabilities. QDS is the most accurate scheme while keeping the number of nodes constant. The accuracy comes with the increase in processing time. LDS is comparable with QDS but have lower accuracy and lower computation time. The combination of UDS1 and QDS is known as the mixed differencing scheme. This method can be used when QDS is unstable and higher stability is required [54].

Number of nodes is selected under this tab as well.

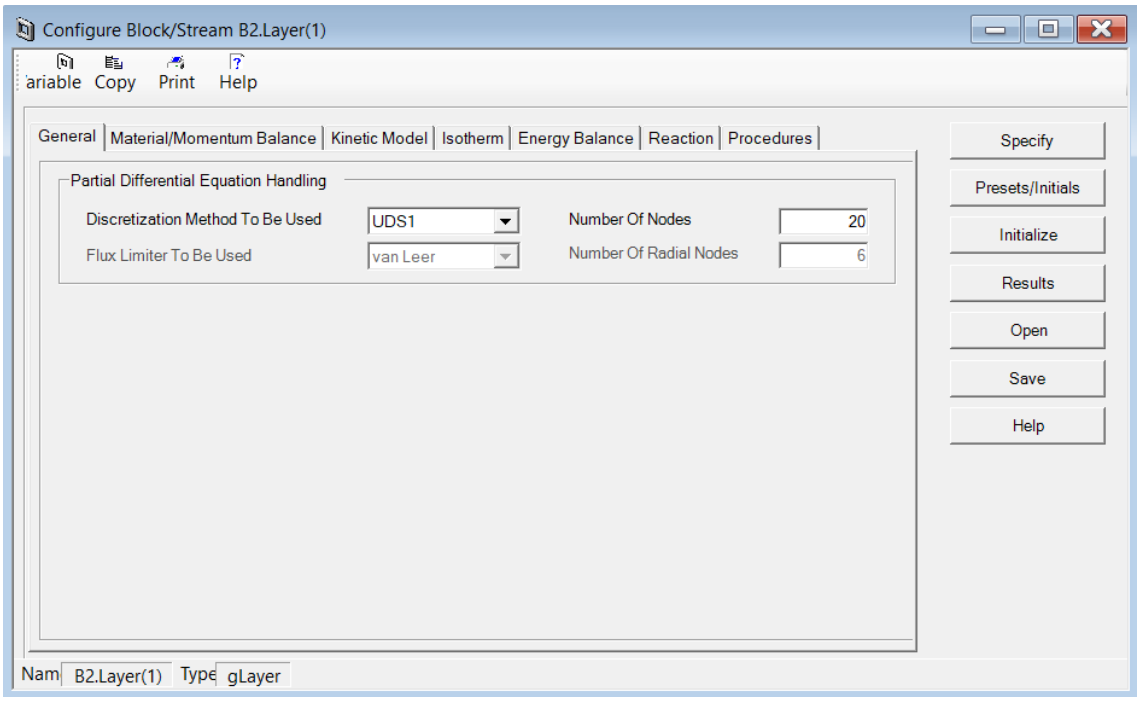

Figure 18. General tab of the configuration window

iv. Next is the "Material/Momentum Balance" tab and it is shown in Figure 19. Several options are available for both the material and momentum balance. Commonly used momentum balance assumption options are Ergun equation, Darcy's law, and the Karman-Kozeny equation.

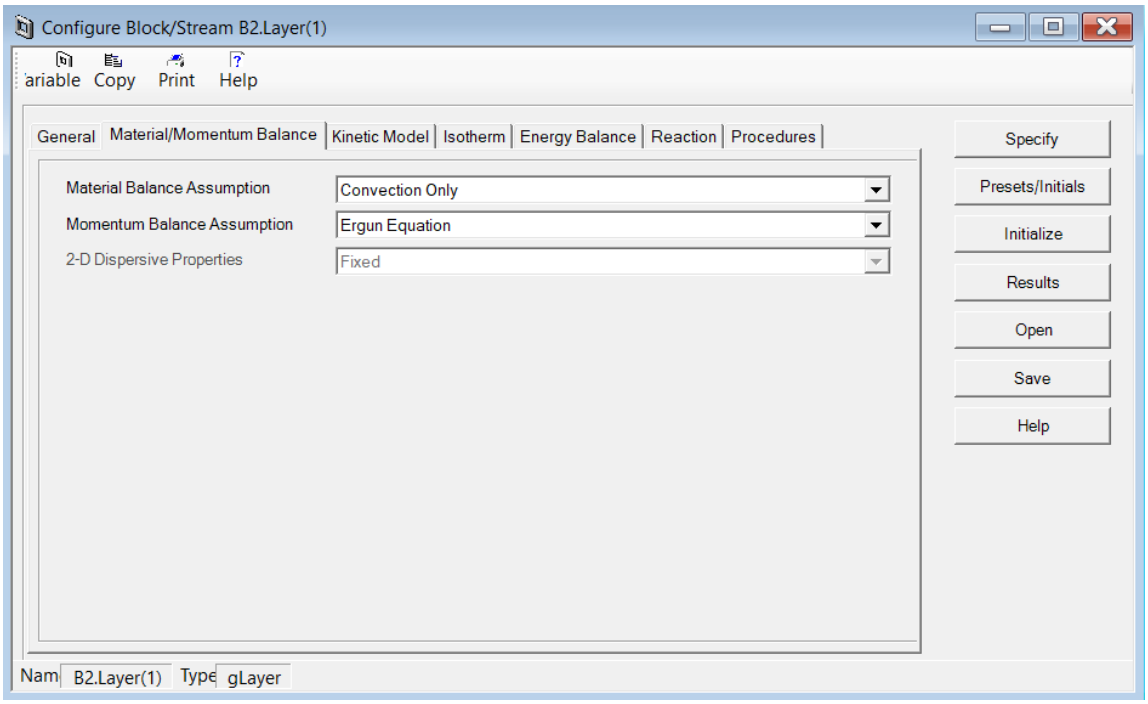

Figure 19. Material/Momentum Balance tab of configuration window

v. Next is the selection of Kinetic Model. The default options are shown in Figure 20. As mentioned in chapter 3.4 that linear lumped resistance model is analogous with the LDF model. The default option is this linear lumped resistance model, and it is the simplest option to choose. The other options for gases are Micro and Macro Pore, Particle MB, Particle MB 2, and the other user specified options.
Micro and macro pore is a good option to choose to get more closer to the practical scenarios. The concentration gradients within the pores and void spaces have a great influence over the rate of diffusion. By providing the mass transfer coefficients for the micro and macro pores, more accurate results can be achieved [54].
Particle MB and particle MB 2 are rigorous methods that solve for particle mass balance to determine the solid loading. More detail about these methods is available in Aspen's help.

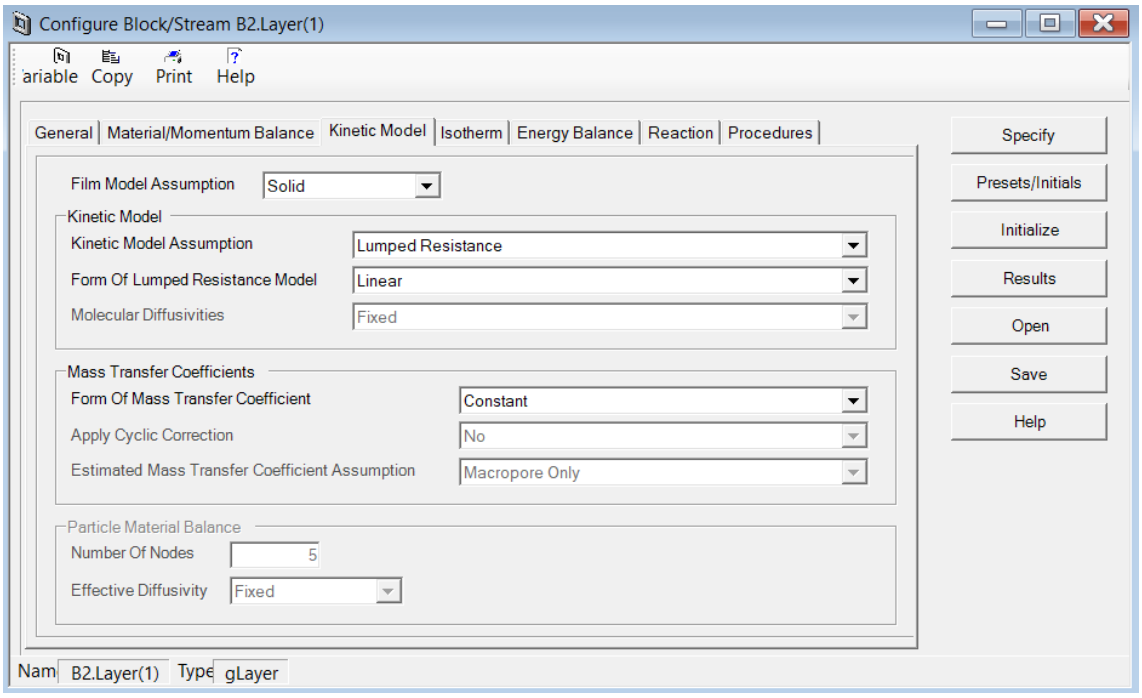

Figure 20. Kinetic Model tab of configuration window

vi. For the Isotherm window, there are 38 available options for the selection of suitable Isotherm type. These isotherms are B.E.T, B.E.T Multilayer, Dual Layer B.E.T, Dual-Site Langmuir, Dual-Site Langmuir 2, Dual-Site Langmuir 2 with I.A.S, Dubinin Astakov, Dubinin-Radushkevich with I.A.S, Extended Langmuir 1, Extended Langmuir 2, Extended Langmuir 3, Extended Langmuir-Freundlich, Freundlich 1, Freundlich 2, Henry 1, Henry 2, I.A.S B.E.T Multilayer, I.A.S Freundlich 1, I.A.S Freundlich 2, I.A.S Henry 1, I.A.S Henry 2, I.A.S Langmuir 1, I.A.S Langmuir 2, I.A.S Langmuir 3, I.A.S Langmuir-Freundlich, Langmuir 1, Langmuir 2, Langmuir 3, Langmuir-Freundlich, Linear, Myers, Single Layer B.E.T, Toth, User Procedure, User Procedure with I.A.S, User Submodel, User Submodel with I.A.S, and Volmer. The details and equations of these isotherms can be found in Aspen Adsorption® help section. Isotherm dependency can be chosen between concentration and partial pressure. Isotherm window is shown in Figure 21.

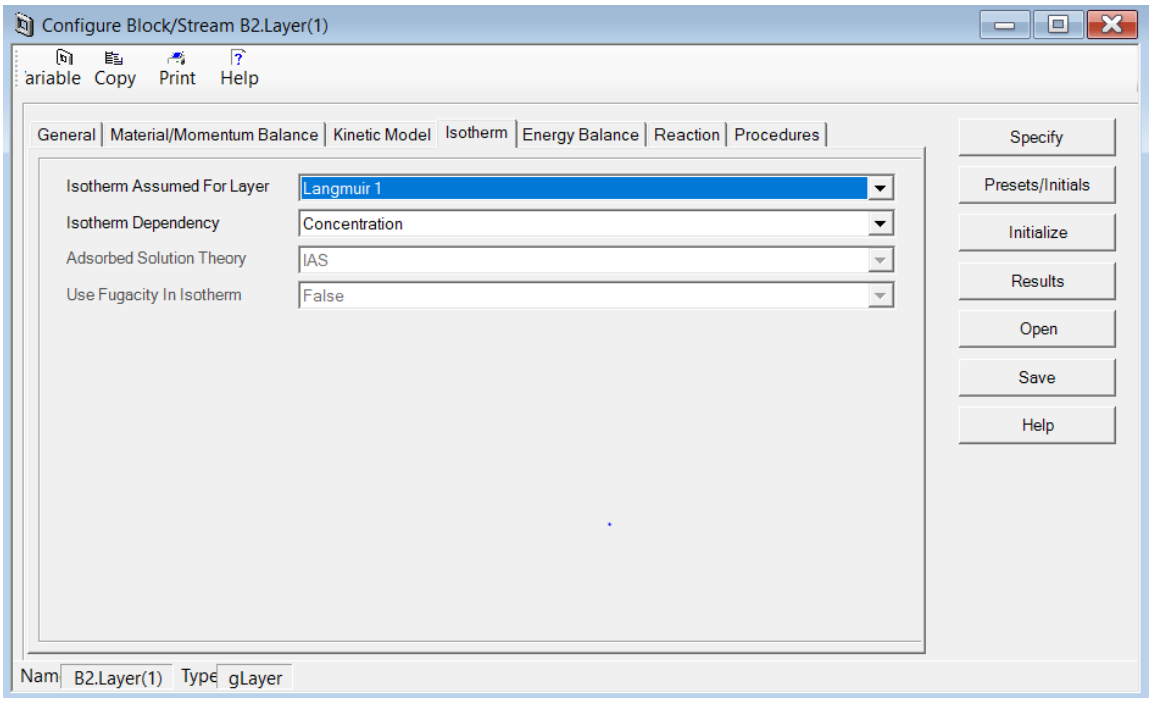

Figure 21. Isotherm tab of configuration window

vii. The default option under the **"Energy Balance"** tab is the Isothermal assumption. In addition to this, there are four non-isothermal options. For non-isothermal options, we need to specify other options such as heat transfer coefficient, and thermal conductivity. This is showed in Figure 22. The next tab **"Reaction"** is for specifying the reaction in case of reactive adsorption. The **"Procedures"** tab is used to provide for user procedures in case we had not chosen components from Aspen Properties. Moreover, it can be used to provide a user specified Isotherm. The common method is by providing your own FORTRAN code.

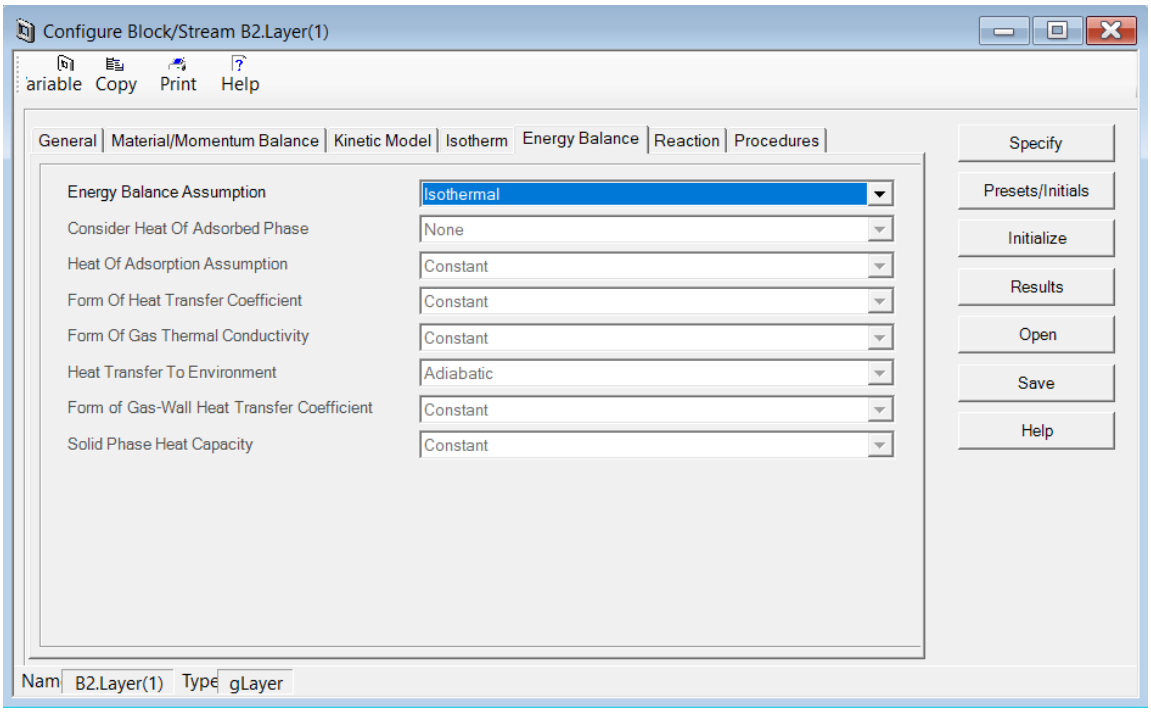

Figure 22. Energy Balance tab of configuration window

4.4 Specifying the Gas_Bed

Next up is giving the specific values for the bed and then to assign initial values for some of the parameters. Click on the **"Specify"** button under the **"Configure Block"** window. This window is shown under Figure 23. These specifications depend on how the bed is configured in the first place. What is shown is the minimum that is needed to be provided.

Then the Figure 24 shows **"Presets/Initials"**. Again, just need to click on this button under the same window. These values are the initial guess for the first node. After giving the initial values. we need to click on the **"Initialize"** button to specify the node 1 values to the remaining nodes.

B1.Layer(1).Specify Table

	Value	Units	Description
Hb	1,0	m	Height of adsorbent layer
Db	0,25	m	Internal diameter of adsorbent layer
Ei	0,42	m3 void/m3 bed	Inter-particle voidage
Ep	0,21	m3 void/m3 bead	Intra-particle voidage
RHOs	592,0	kg/m3	Bulk solid density of adsorbent
Rp	1,e-003	m	Adsorbent particle radius
SFac	1,0	n/a	Adsorbent shape factor
Direction	0,0	n/a	Specified flow direction (self determined: 0, forward: 1)

Figure 23. Specifications for Gas_Bed

B2.Layer(1).Initials_YVWC Table

	Value	Units	Spec	Derivative	Description
ProfileType	Constant				Is the bed initially specified with constant or
Y_First_Node(*)					
Y_First_Node("NITROGEN")	0,5	kmol/kmol	Initial		Mole fraction within first element
Y_First_Node("WATER")	0,5	kmol/kmol	Initial		Mole fraction within first element
Vg_First_Node	3,55e-004	m/s	Initial		Gas velocity within first element
W_First_Node(*)					
W_First_Node("NITROGEN")	0,0	kmol/kg	RateInitial	0,0	Solid loading within first element
W_First_Node("WATER")	0,0	kmol/kg	RateInitial	0,0	Solid loading within first element

Figure 24. Presets/Initials window of Gas_Bed

4.5 Cycle organizer

Cycle organizer is the tool used to create the steps that define a cyclic process such as TSA or PSA. Number of different steps can be created to represent each stage in the process. End of the step can be based on an event such as bed reaching a certain temperature or pressure. Step can also be terminated simply by specifying an end of step time.

Each step in the cycle can be specified with manipulated variables such as flowrate, pressure, and temperature. It is better to install valves for the streams for which flowrates are to be manipulated.

Cycle organizer is used in the case of TSA for biogas under Chapter 5.3. It can be seen in Table 20 that how different flowrates and temperatures are assigned for several steps in a TSA process.

APPLIED PART

5 ASPEN SIMULATIONS

In this chapter, number of different adsorption cases are modelled and simulated to better understand the capabilities of Aspen Adsorption software. These cases include nitrogen/oxygen separation, methane and carbon dioxide separation from biogas, methane and carbon dioxide separation with TSA cycle, and water adsorption.

5.1 Nitrogen/Oxygen separation

This simulation is carried out to demonstrate the possibility of using Aspen Adsorption® for the DAC of carbon dioxide. For this simulation, the simplest possible configuration is used. The process flowsheet for this process just contains three blocks. These blocks are feed, product, and the gas_bed. Figure 25 shows the process flowsheet for this simulation.

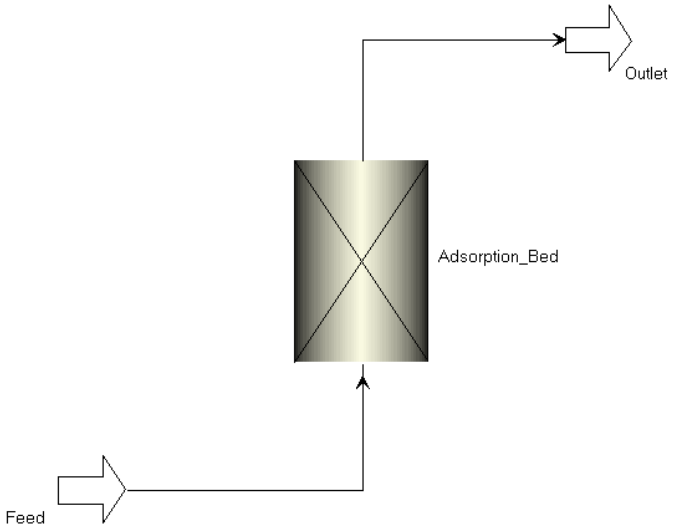

Figure 25. Flowsheet for the process

For the bed specifications again, the simplest possible specifications are used, and they are given in Table 5. Isotherm and mass transfer data is taken from the article by Tian et al [83]. Extended Langmuir 2 is chosen as the isotherm model, and it is given in Eq. 3.6 in chapter 3.

Table 7. Specifications used for the bed

Specification type	Specification	Selected option
General	Discretization Method to be used	UDS1
	Number of Nodes	20

Continuation of Table 7.

Material/ Momentum Balance	Material Balance Assumption	Convection Only
	Momentum Balance Assumption	Karman-Kozeny
Kinetic Model	Film Model Assumption	Solid
	Kinetic Model Assumption	Lumped Resistance
	Form of Lumped Resistance Model	Linear
	Form of Mass Transfer Coefficient	Constant
Isotherm	Isotherm Assumed for Layer	Extended Langmuir 2
	Isotherm Dependency	Partial Pressure
Energy Balance	Energy Balance Assumption	Isothermal

Tables 7 and 8 gives the parameters used for this simulation. Some of these parameters such as flowrate are manipulated over a range of values to get the simulation running over a suitable period of time. The simulation was completed in 5000 seconds for the flowrate used. The flowrate for the feed is given in Table 10.

The adsorbent used is LiLSX zeolite. This is also modelled according to the article by Tian et al [83].

Table 8. Constant parameters used for the bed

Specification (units)	**Value**
Height of adsorbent layer (m)	0.35
Internal diameter of adsorbent layer (cm)	3.5
Inter-particle voidage (m3 void/ m3 bed)	0.64
Intra-particle voidage, (m3 void/ m3 bead)	0.53
Bulk solid density of adsorbent (kg/m3)	641.0
Adsorbent particle radius (mm)	1.055
Adsorbent shape factor (n/a)	1.0
Constant mass transfer coefficient Nitrogen (1/s)	2.05
Constant mass transfer coefficient Oxygen (1/s)	4.98

Table 9. Isotherm parameters for the bed

Isotherm parameters (Units)	**Value**
IP1 Nitrogen (kmol/ kg bar)	7.107×10^{-5}
IP1 Oxygen (kmol/kg bar)	6.861×10^{-4}
IP2 Nitrogen (K)	2910

Continuation of Table 9.

IP2 Oxygen (K)	1567
IP3 Nitrogen (1/bar)	2.563×10^{-3}
IP3 Oxygen (1/bar)	4.625×10^{-3}
IP4 Nitrogen (K)	1612
IP4 Oxygen (K)	441.3

It was assumed that bed is filled with nitrogen before the oxygen is fed to the bed. For this the initial mole fraction of nitrogen is given the value 1.0. Solid loading for both the nitrogen and oxygen is 0.0. These presets are given in table 8.

Table 10. Values and specifications for the 1st node of the bed

Node Description	Specification	Value
Mole fraction within first element, Nitrogen (kmol/kmol)	Initial	1.0
Mole fraction within first element, Oxygen (kmol/kmol)	Initial	0.0
Solid loading within first element, Nitrogen (kmol/kg)	Rateinitial	0.0
Solid loading within first element, Oxygen (kmol/kg)	Rateinitial	0.0

Tables 9 and 10 give the feed and product specifications. Both the feed and the product are at room temperatures. The feed compositions are chosen such as to represent the compositions in the air.

Table 11. Feed specification and values

Description (Units) Feed	Specification	Value/Type
Model type		Reversible pressure setter
Flowrate (kmol/s)	Fixed	3×10^{-5}
Composition in forward direction, Nitrogen (kmol/kmol)	Fixed	0.79
Composition in forward direction, Oxygen (kmol/kmol)	Fixed	0.21
Temperature in forward direction (K)	Fixed	298.15
Boundary pressure (bar)	Fixed	3.045

Table 12. Product specification and values

Description (Units) Product	Specification	Value/Type
Model type		Reversible pressure setter
Flowrate (kmol/s)	Free	Pressure drop dependent
Composition in reverse direction, Nitrogen (kmol/kmol)	Fixed	0.5
Composition in reverse direction, Oxygen (kmol/kmol)	Fixed	0.5
Temperature in forward direction (K)	Fixed	298.15
Boundary pressure (bar)	Free	

In Figure 26 we can observe how the composition of nitrogen and oxygen changes over time. For about the first 250 seconds the oxygen is completely adsorbed on to the bed. Then it gradually decreases to 0.8 kmol/kmol between 250 and 2750 seconds. This can be observed by the outlet composition of the streams and for oxygen it is 0.2 kmol/kmol. After that, the compositions remain constant.

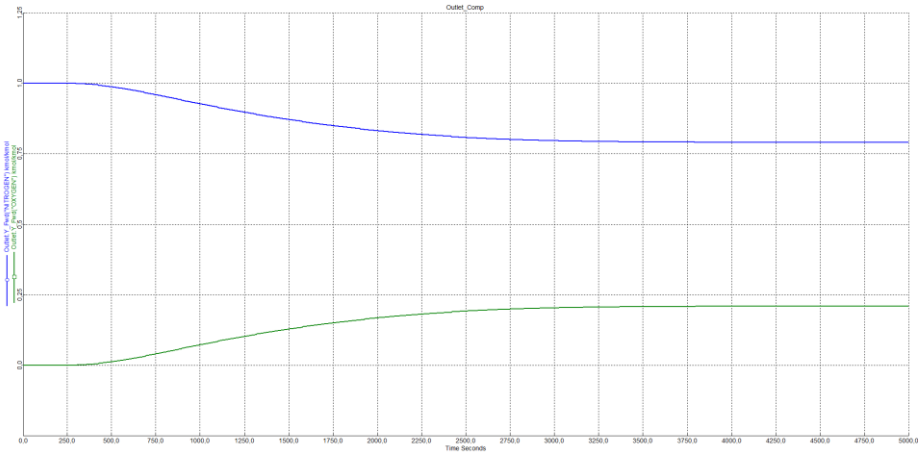

Figure 26. Change in composition of product stream with time

Figure 27 shows the breakthrough curve for oxygen. The final composition is a little over 0.205 kmol/kmol. The curve shape is characteristic of a wide mass transfer zone.

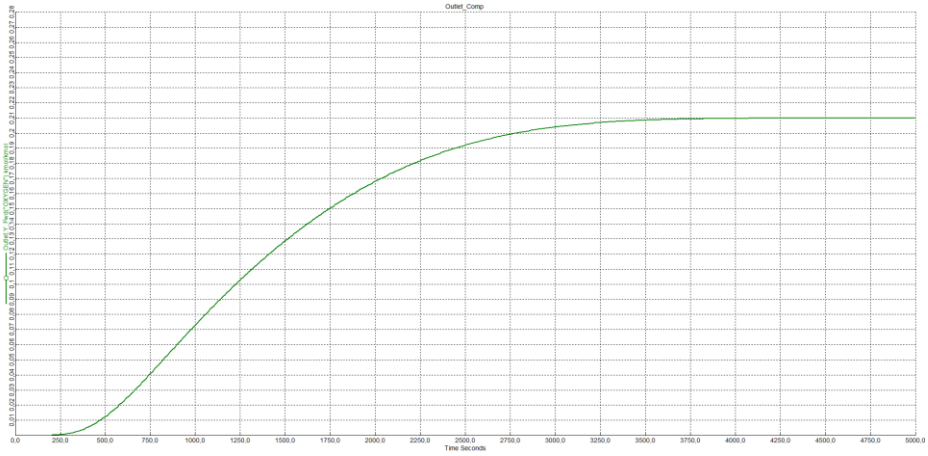

Figure 27. Breakthrough curve for Oxygen

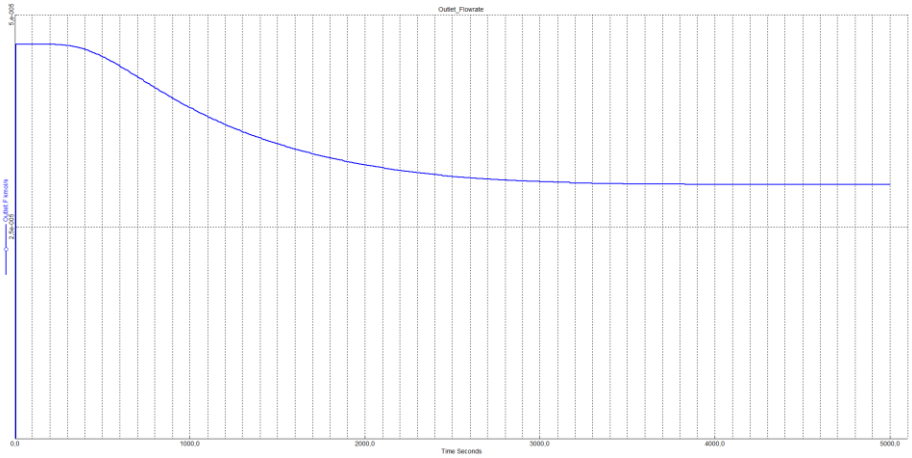

Figure 28. Change in product flowrate with time

Figure 28 shows the change in the product stream flowrate. The whole process operates at a very low flowrate, and the important thing to notice is the gradual decrease in the flowrate until about 3000 seconds. After that the flowrate becomes constant as no further adsorption takes place. The considerable increase in the flowrate in the beginning of the process is because of the rapidly desorbing nitrogen that is present in the column.

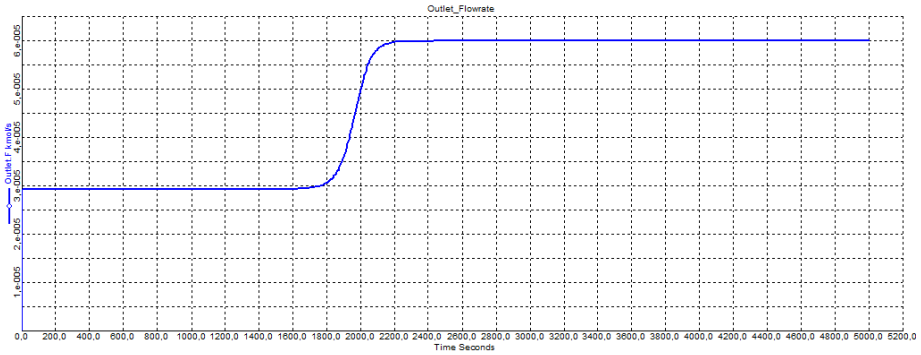

Figure 29. Change in product flowrate with time for an empty bed (validation run)

Figure 29 is also for the change in product stream flowrate, but with a bed initially empty. This is for the validation of the results of the simulation. The trend shown is the usual and the expected for the exit flowrate of the adsorption column. The flowrate is constant at a very low value since all the oxygen from the feed is being adsorbed for the first 1800 seconds.

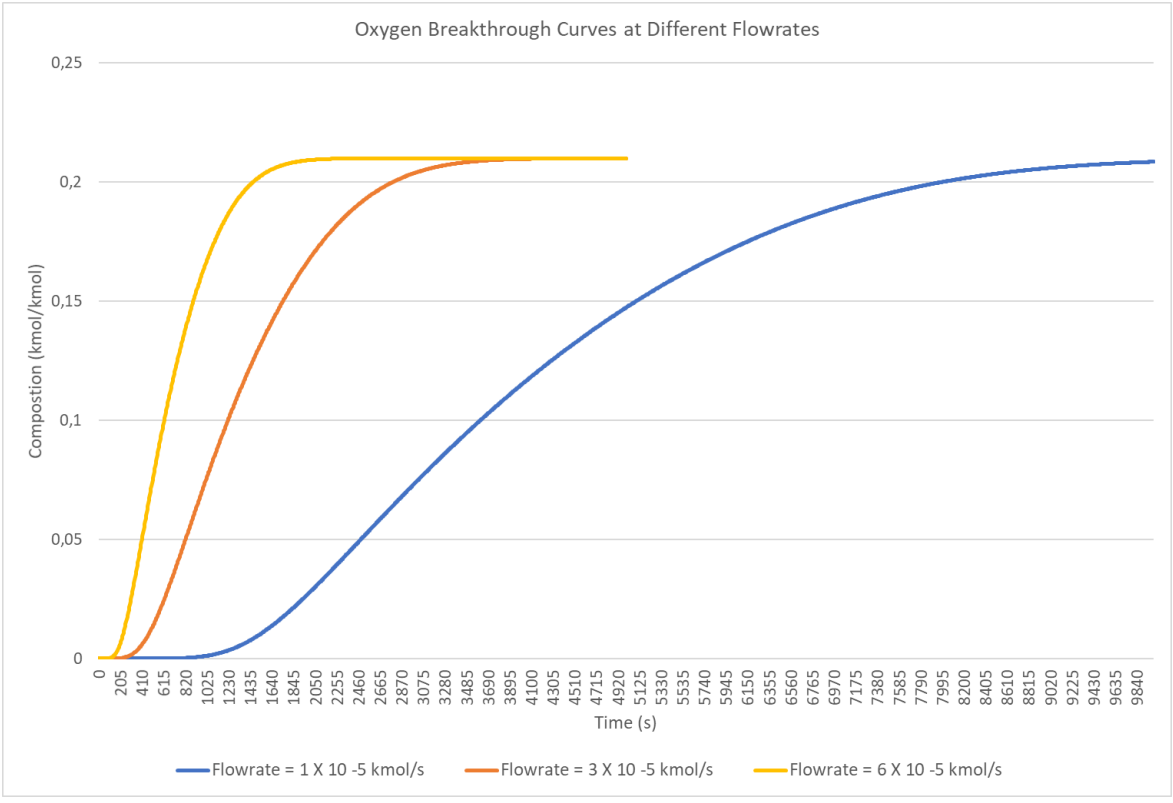

Figure 30. Breakthrough curve comparison at different flowrates

Figure 30 represents the three different breakthrough curves at three different flowrates. The orange curve is for the initial settings with a flowrate of 3×10^{-5}. The trend shows that by decreasing the flowrate to 1×10^{-5} more time is taken to reach the equilibrium value, but the mass transfer zone is spread out across the bed. This also means that adsorption takes place for more time at a lower flowrate.

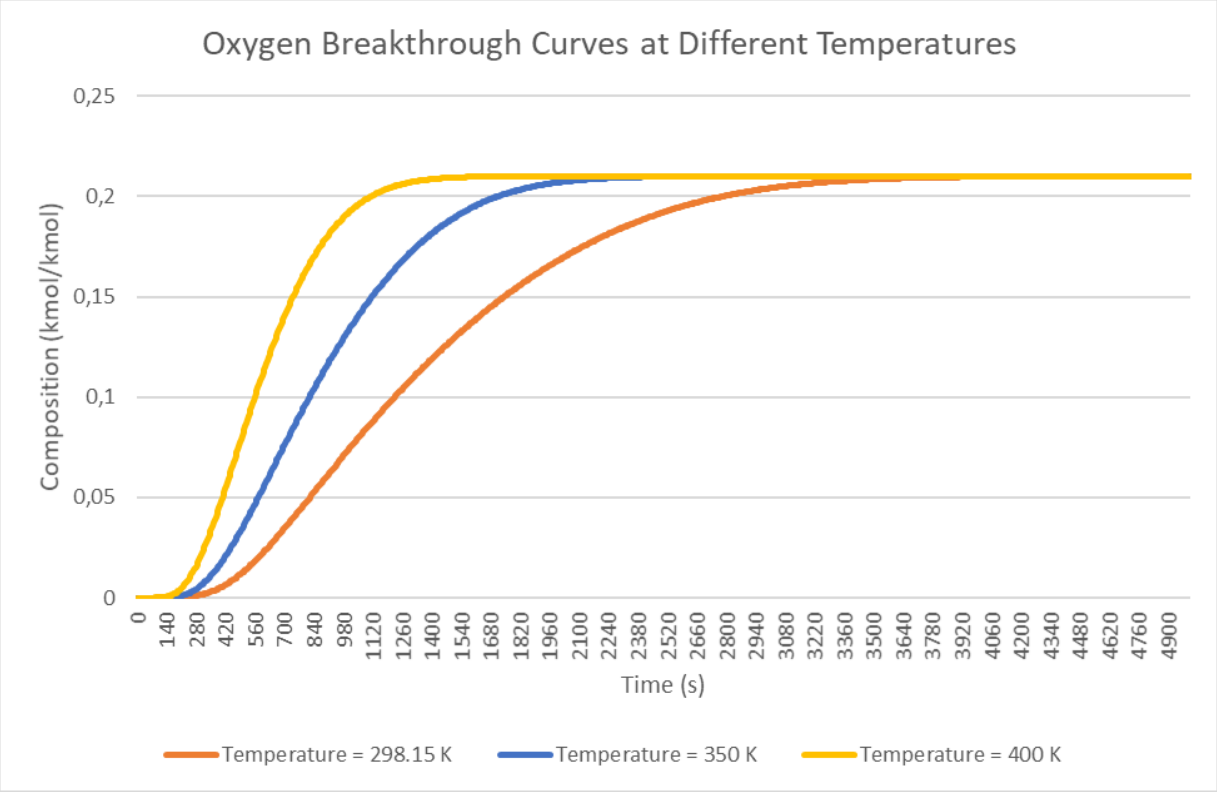

Figure 31. Breakthrough curve comparison at different temperatures

Figure 31 shows the trend of oxygen breakthrough curves with temperature. Increasing the decreases the time taken to reach the constant value, and that means oxygen is adsorbed for shorter time than at a lower temperature. Also, the mass transfer zone is more spread out at a lower temperature.

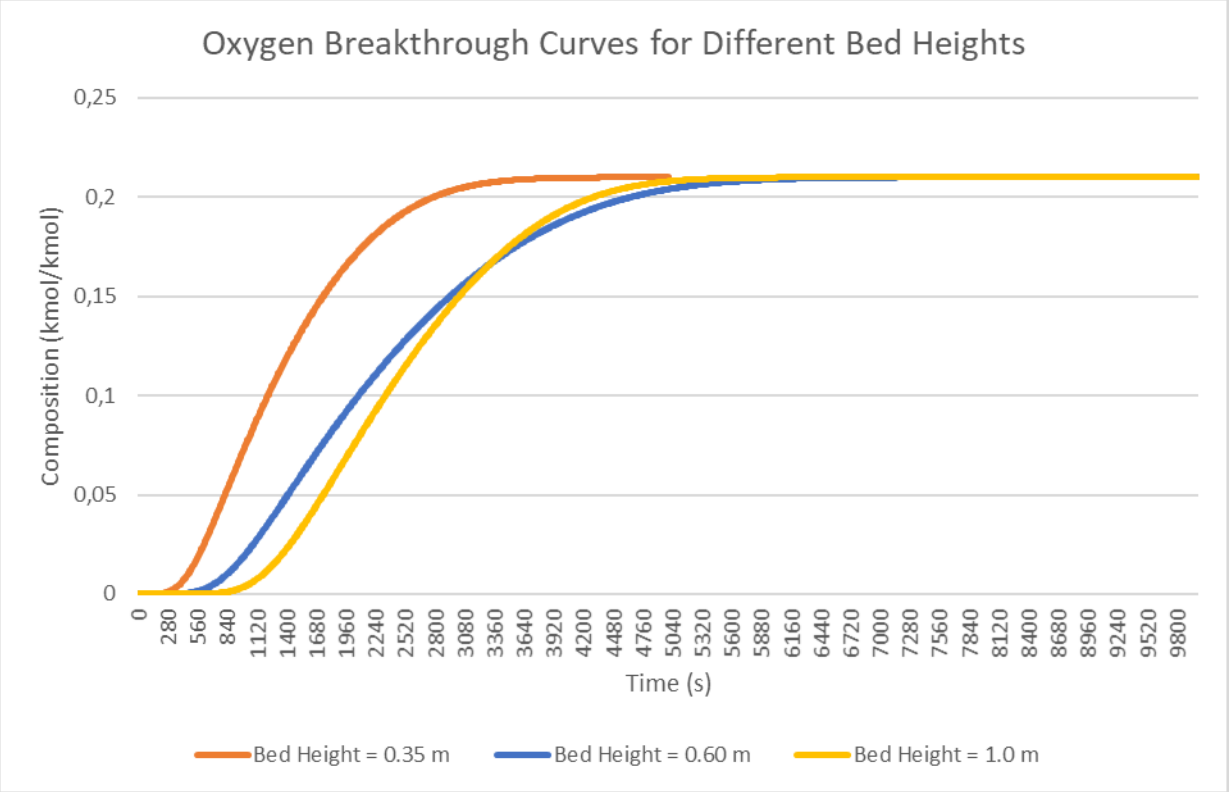

Figure 32. Breakthrough curve comparison for different bed heights

Figure 32 shows how the breakthrough curve changes with varying bed height. The trend shows that increasing the bed height increases the time taken for adsorption, in other words more oxygen is adsorbed. The shape for bed height of 1m also shows that mass transfer zone is also a little more spread across the bed.

5.2 Methane and Carbon dioxide separation from Biogas

This simulation is carried to test capabilities of Aspen Adsorption® for the biogas case. Process flowsheet for this process is given in Figure 33. It is like the last case with the addition of control valves.

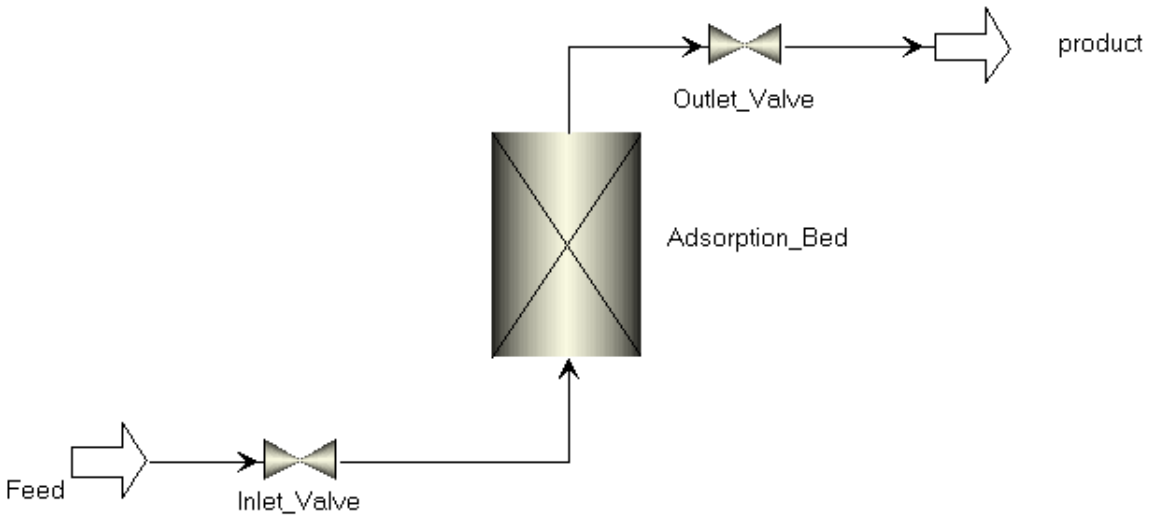

Figure 33. Flowsheet for the process

This simulation is modelled according to the tutorial video available online by Tavan [84].

The specifications for the simulation are given in Table 13. Dispersion is considered in this case for the mass balance assumption. Extended Langmuir 2 is chosen as the isotherm model and is given in Eq. 3.6 in chapter 3.

For energy balance, non-isothermal case is taken. Conduction is considered between solid and gas phase. Adiabatic heat transfer to the environment is assumed.

Table 13. Specifications used for the bed

Specification type	**Specification**	**Selected option**
General	Discretization method to be used	UDS1
	Number of Nodes	20
Material/ Momentum Balance	Material Balance Assumption	Convection with estimated dispersion
	Momentum Balance Assumption	Ergun equation
Kinetic Model	Film Model Assumption	Solid
	Kinetic Model Assumption	Lumped Resistance
	Form of Lumped Resistance Model	Linear
	Form of Mass Transfer Coefficient	Constant

Continuation of Table 13.

Isotherm	Isotherm Assumed for Layer	Extended Langmuir 2
	Isotherm Dependency	Partial Pressure
Energy Balance	Energy Balance Assumption	Non-isothermal with gas and solid conduction
	Heat transfer to environment	Adiabatic

The bed specifications are given in Table 14 and a silicate adsorbent is chosen for this case. Higher mass transfer values are taken just for simulation to reach the equilibrium quicker. CO_2 value is much higher compared to CH_4 since CO_2 is adsorbing strongly, this helps with simulation running faster. Isotherm values are given in Table 15.

Table 14. Constant parameters used for the bed

Specification (units)	**Value**
Height of adsorbent layer (m)	0.163
Internal diameter of adsorbent layer (cm)	1.6
Inter-particle voidage (m3 void/ m3 bed)	0.52
Intra-particle voidage (m3 void/ m3 bead)	0.59
Bulk solid density of adsorbent (kg/m3)	515.93
Adsorbent particle radius (mm)	0.7
Adsorbent shape factor	1.0
Constant mass transfer coefficients CH_4 (1/s)	5.0
Constant mass transfer coefficients CO_2 (1/s)	110
Adsorbent specific heat capacity (J/kg/K)	1000
Constant heat of adsorption for CH_4 (J/kmol)	$-1.8 \times 10^{+7}$
Constant heat of adsorption for CO_2 (J/kmol)	$-2.26 \times 10^{+7}$
Constant for the gas phase heat conductivity (W/m/K)	0.025
Adsorbent thermal conductivity (W/m/K)	0.6
Specific surface area of adsorbent (1/m)	2057.14

Table 15. Isotherm parameters for the bed

Isotherm parameters (Units)	**Value**
IP1 CH_4 (kmol/ kg bar)	6.31×10^{-6}
IP1 CO_2 (kmol/ kg bar)	1.27×10^{-5}
IP2 CH_4 (K)	1056

Continuation of Table 15.

IP2 CO_2 (K)	1187
IP3 CH_4 (1/bar)	4.7×10^{-5}
IP3 CO_2 (1/bar)	1.23×10^{-4}
IP4 CH_4 (K)	1067
IP4 CO_2 (K)	1210

Initial 1st node values of the bed are given in Table 16. It is assumed the bed is already filled with methane. Then the feed and product stream specifications are given in Table 17 and Table 18, respectively. It is important to notice that flowrates are not specified and are rather controlled by the control valves. The control valve specifications are given in Table 19.

Table 16. Values and specifications for the 1st node of the bed

Node Description (Units)	**Specification**	**Value**
Mole fraction within first element, CH_4 (kmol/kmol)	Initial	1.0
Mole fraction within first element, CO_2 (kmol/kmol)	Initial	0.0
Solid loading within first element, CH_4 (kmol/kg)	Rateinitial	0.0
Solid loading within first element, CO_2 (kmol/kg)	Rateinitial	0.0

Table 17. Feed specification and values

Description (Units)	**Specification**	**Value/Type**
Model type		Reversible pressure setter
Flowrate (kmol/s)	Free	
Composition in forward direction, CH_4 (kmol/kmol)	Fixed	0.62
Composition in forward direction, CO_2 (kmol/kmol)	Fixed	0.38
Temperature in forward direction (K)	Fixed	290.0
Boundary pressure (bar)	Fixed	10

Table 18. Product specification and values

Description (Units)	**Specification**	**Value/Type**
Model type		Reversible pressure setter
Flowrate (kmol/s)	Free	
Composition in reverse direction, CH_4 (kmol/kmol)	Fixed	1.0
Composition in reverse direction, CO_2 (kmol/kmol)	Fixed	0.0
Temperature in forward direction (K)	Fixed	290.0
Boundary pressure (bar)	Free	9.95

Table 19. Valve specifications for inlet and outlet

Specifications	**Inlet Valve**	**Outlet Valve**
Active specification	3.0	1.0
Cv (kmol/s/bar)	100.0	100.0
Flowrate (kmol/s)	8×10^{-7}	0.05

The breakthrough curve for CO_2 is given in Figure 34. Since a rather large value is selected for the mass transfer coefficient of CO_2, the breakthrough point is around 70 seconds that is very quick for such a process. The curve has a gradual slope, and it is spread over the whole process, indicating wide range of mass transfer zone and the unutilized capacity of the bed.

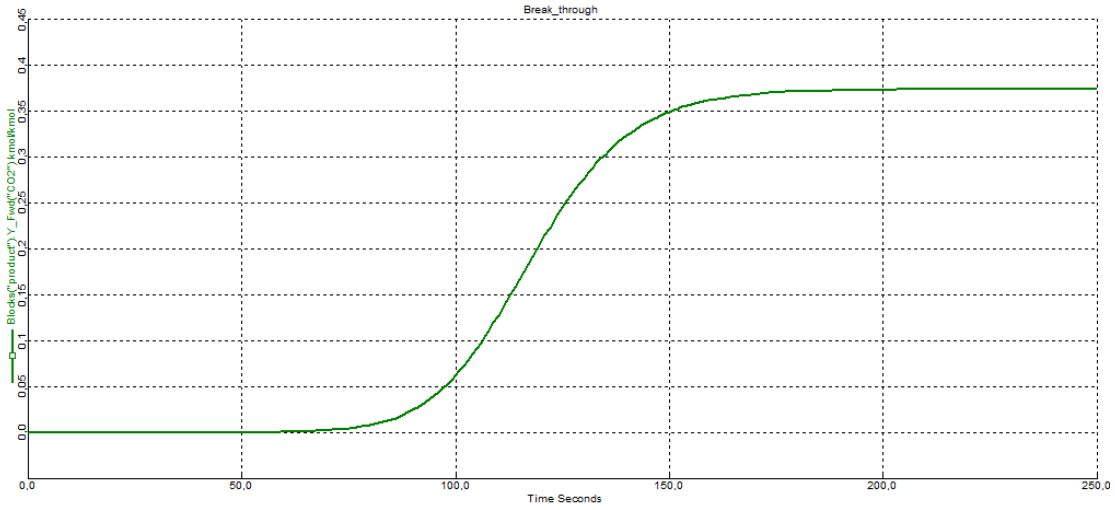

Figure 34. Breakthrough curve for CO_2

CO_2 loading at different node positions is compared with the 1st node loading of CH_4 in the Figure 35. There is a sharp decline in the value of methane from about 0.022 kmol/kg as soon as the feed is fed. The maximum loading achieved for CO_2 is around 0.023 kmol/kg. The red

curve is for CO_2 loading at node position 5, the green at position 10, and blue at position 20. The red curve represents the position close to the entrance of the bed, that is the reason it reached equilibrium before the other node positions, and the curve is towards the left, but with the same shape.

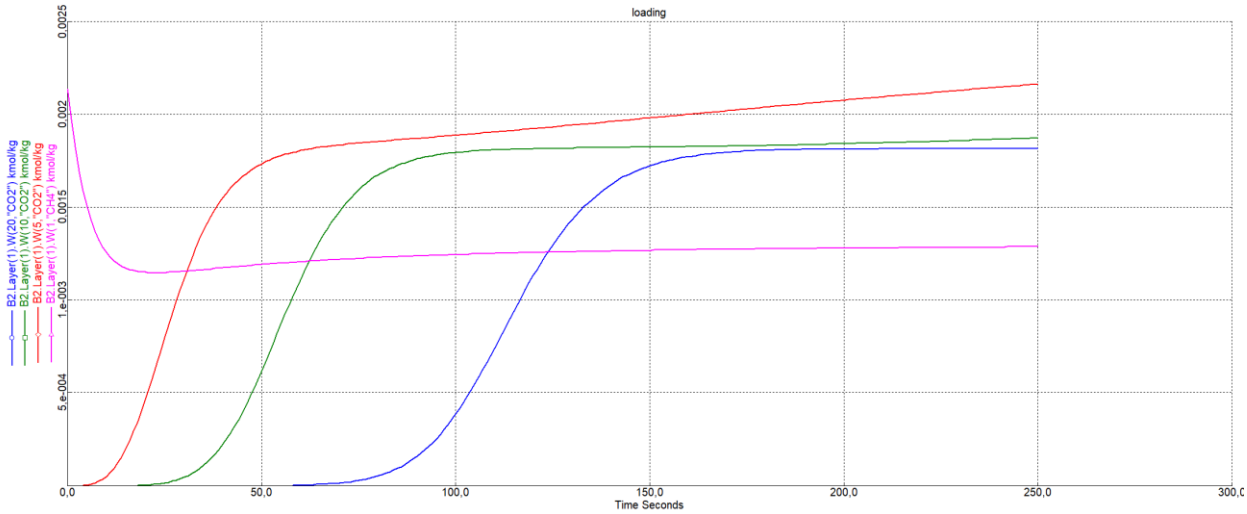

Figure 35. CO_2 loading at different points compared with CH_4 loading

As indicated before that the mass transfer zone is well spread out, this can be better visualized in Figure 36. The x-axis shows the length of the column. For the beginning of the process and close to the breakthrough point, the mass transfer zone is widely spread over the whole the bed. This is indicated by the curves at time 50 and80 seconds. After 130 seconds most of the bed is saturated with CO_2.

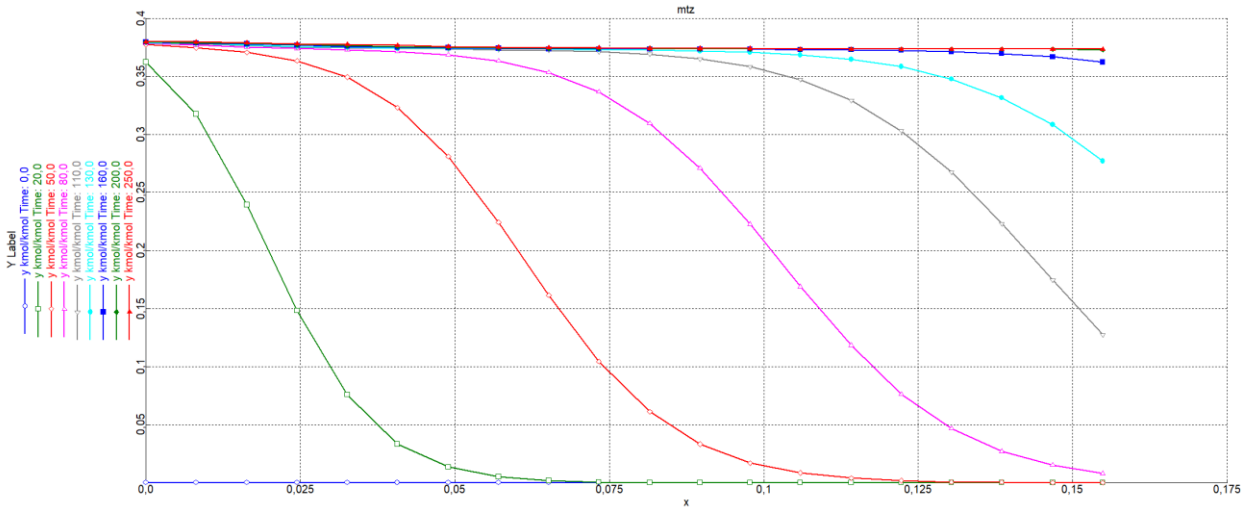

Figure 36. Mass transfer zones at different times with respect to position in bed

5.3 Methane and Carbon dioxide separation from Biogas with TSA cycle

In this case the same flowsheet and parameters are used as in the last simulation of a simple once through separation of methane and oxygen. These parameters are given in Tables 13-19. In this simulation a cycle organizer is used to essentially vary the temperature of the bed to desorb the adsorbed gasses.

5.3.1 Cycle organizer

Cycle organizer is used to run the simulation in three steps. The first step is adsorption, second is heating and the last step is cooling of the bed. Cooling is added to get the bed back to the optimum temperature for adsorption step.

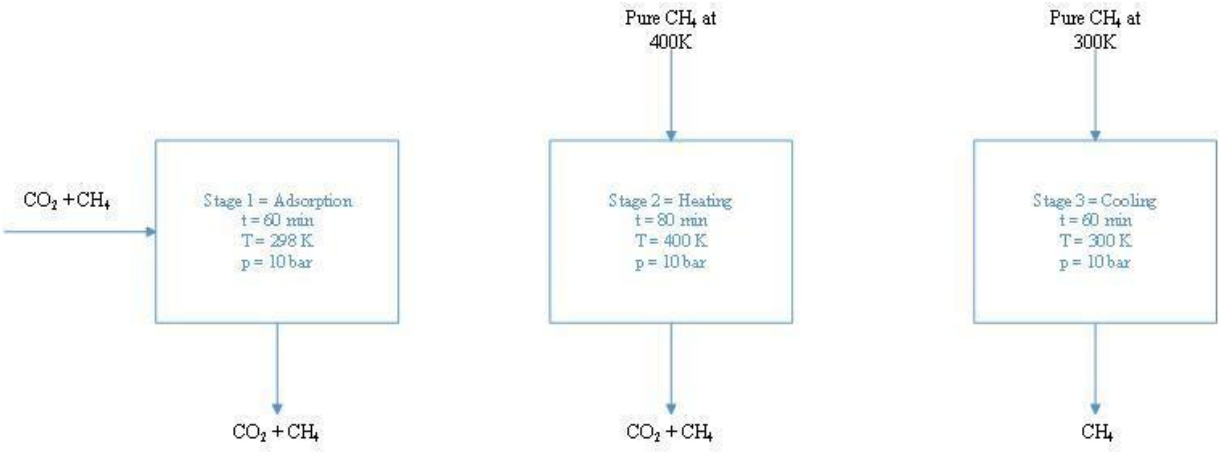

Figure 37. Block diagram for cyclic TSA Process

Figure 37 shows the block diagram for the process to better explain the setup of cycle organizer. The block diagram shows three different processes occurring in the same adsorption column. The first stage runs for 60 min at 298 K and 10 bars. At this stage most of the CO_2 is adsorbed. Stage 2 is the desorption step, where column is heated to 400 K with pure methane stream. Both the CO_2 and CH_4 comes out of the system in this step. The last step is to bring down the temperature for the adsorption step, this is also done with the help of pure methane stream, and since all the CO_2 is desorbed in the 2^{nd} stage, only CH_4 comes out of the system. The times chosen are to provide enough time for adsorption, heating, and cooling but are not optimized.

Table 20. Variables and their values for different steps of TSA in cycle organizer

Manipulated variables	**Stage 1: Adsorption**	**Stage 2: Heating**	**Stage 3: Cooling**
	Time: 60 min	**Time: 80 min**	**Time: 60 min**
Feed valve: active specification	3	3	3
Feed valve: Flowrate (kmol/s)	8×10^{-7}	2×10^{-7}	2×10^{-7}
Outlet valve: active specification	1.0	1.0	1

Continuation of Table 20.

Feed pressure (bar)	10.0	10.0	10.0
Feed temperature (K)	298.0	450.0	300.0
Composition in forward direction CH_4 (kmol/kmol):	0.62	1.0	1.0
Composition in forward direction CO_2 (kmol/kmol):	0.38	0.0	0.0

Temperature variation of the TSA cycle is shown in Figure 38 for three different node positions. Logically the first node, that is the entrance of the bed achieves the desired temperature before the positions further away. Longer time duration is chosen compared to once through case to help with achieving of the desired temperatures. Heating of the bed is achieved rather instantaneously, and sensible approach would be to reduce the time for heating. This cannot be done since enough time is required to desorb all the CO_2 present in the bed. This is shown in Figure 39 that shows a quite a gradual curve for the desorption. This is shown in the rising part of the curve. For cooling, it is clear that it is very gradual, and it cannot be achieved any faster. Node 1 is chosen for CH_4, since that represents the maximum holdup of CH_4. For CO_2 last node is taken to again compare the maximum value for both the species.

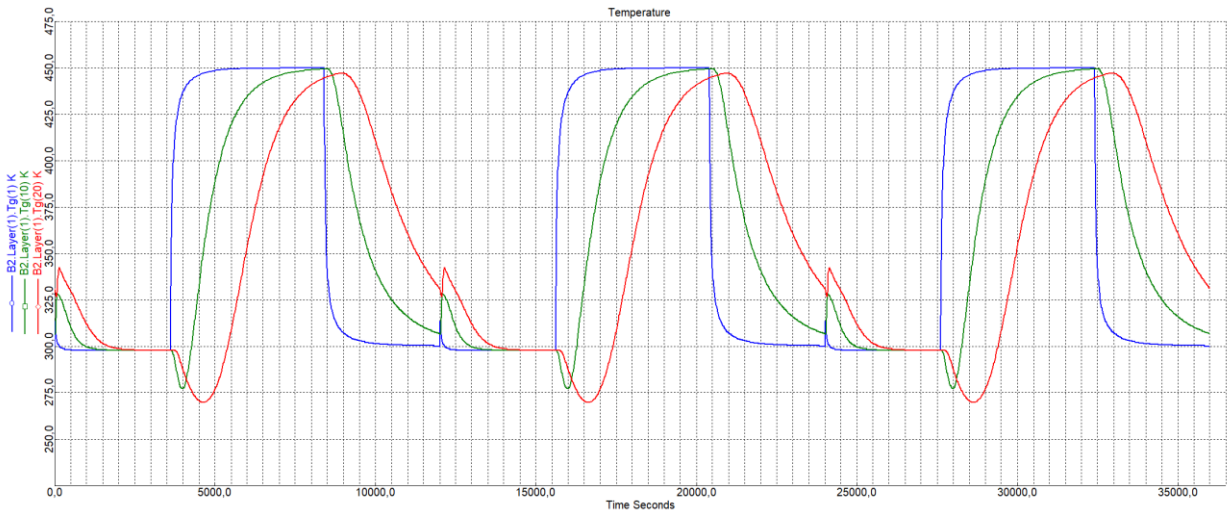

Figure 38. Temperature variation with time at different nodes

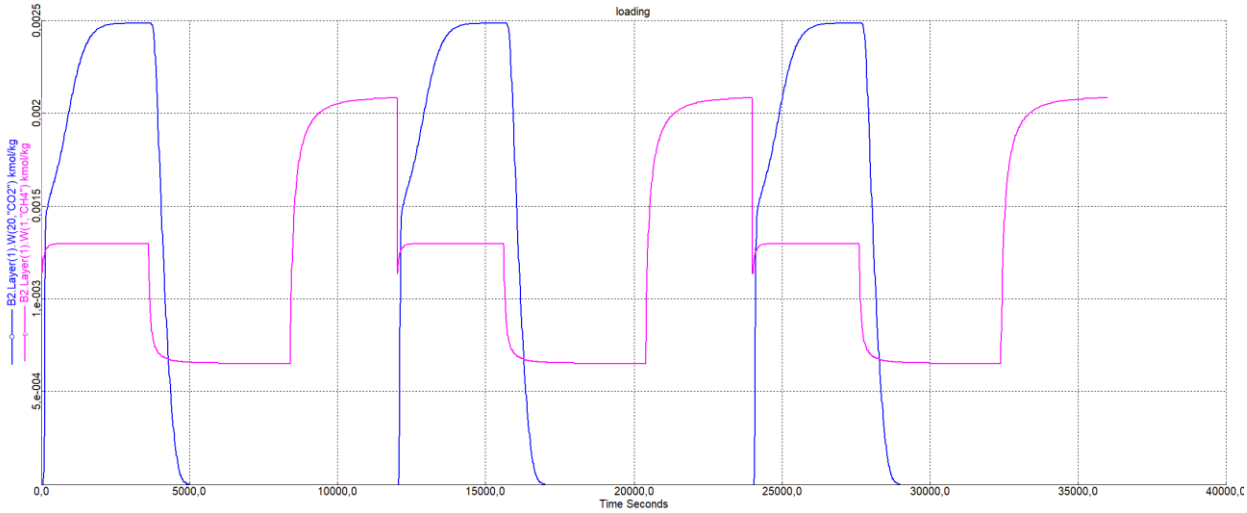

Figure 39. Loading variation with time for CO_2 and CH_4

Figure 40 shows the variation in product stream. This helps us understand that the cyclic process is working properly. The upward trend of the CO_2 curve and the constant straight line indicates the adsorption, and the downwards slope is for desorption step. The time where no CO_2 comes out is for both the cooling and heating steps. Cycle lengths are not optimized in this case.

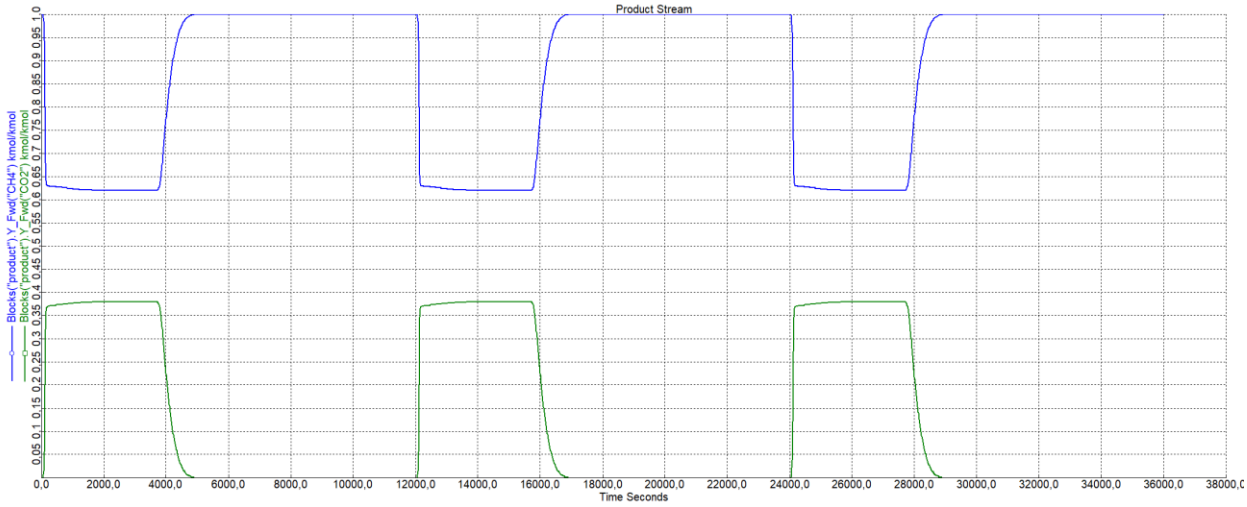

Figure 40. Change in composition of product stream with time

5.4 Water Adsorption

Water adsorption is an important part of flue gas separation. Water usually hinders the adsorption of other gases such as CO_2 in the stream. Therefore, it is important to remove water before we can move on to adsorb/separate other gases. A simple case for water adsorption is

taken in this section to test the suitability of Aspen Adsorption®. Figure 41 shows the simple flowsheet of the process, that consists of one adsorption column, inlet, and the outlet stream.

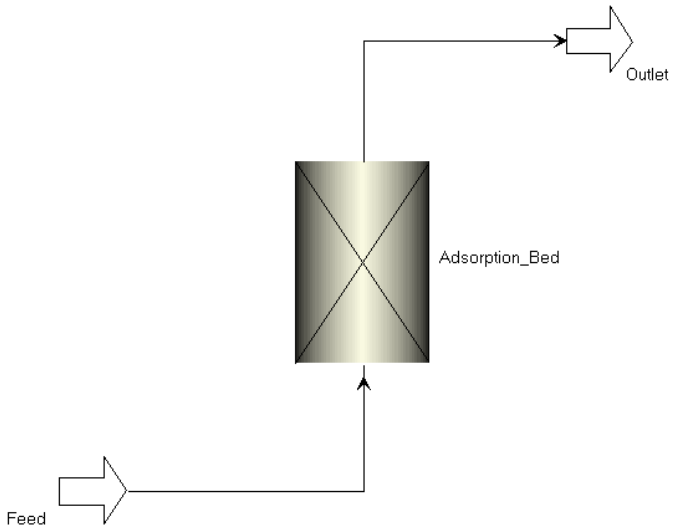

Figure 41. Flowsheet of the process

Most of the options chosen for the bed specifications are the default options and are given in Table 21. Number of nodes were increased to 40 to get more accurate results with Langmuir 1. System is assumed to be isothermal.

Table 21. Specifications used for the bed

Specification type	**Specification**	**Selected option**
General	Discretization Method To Be Used	UDS1
	Number of Nodes	40
Material/ Momentum Balance	Material Balance Assumption	Convection Only
	Momentum Balance Assumption	Karman-Kozeny
Kinetic Model	Film Model Assumption	Solid
	Kinetic Model Assumption	Lumped Resistance
	Form of Lumped Resistance Model	Linear
	Form of Mass Transfer Coefficient	Constant
Isotherm	Isotherm Assumed for Layer	Langmuir 1
	Isotherm Dependency	Partial Pressure
Energy Balance	Energy Balance Assumption	Isothermal

Bed parameters are given in Table 22 and 23. The adsorbent modelled for this simulation is zeolite 3A. This simulation is based on the data collected from the article by Wang et al [58]. In their study, triple-site Langmuir was used to increase the accuracy. Same water isotherm parameter values were taken from the article, but for the sake of simplicity Langmuir 1 is used. Langmuir 1 is of same type but has a larger error.

Mass transfer coefficient value for water is taken as 5 $s^{-1.}$ This value is selected for demonstration purposes without any detailed knowledge of mass transfer in this case. The value is high and therefore the system reaches equilibrium quickly.

The initial node values are given in Table 24.

Table 22. Constant parameters used for the bed

Specification (units)	**Value**
Height of adsorbent layer (mm)	350
Internal diameter of adsorbent layer (mm)	10
Inter-particle voidage (m3 void/ m3 bed)	0.42
Intra-particle voidage (m3 void/ m3 bead)	0.0
Bulk solid density of adsorbent (kg/m3)	592.0
Adsorbent particle radius (mm)	1.0
Adsorbent shape factor	1.0
Constant mass transfer coefficients, Nitrogen (1/s)	0.0076
Constant mass transfer coefficients, Water (1/s)	5.0

Table 23. Isotherm parameters for the bed

Isotherm parameters (Units)	**Value**
IP1 Nitrogen (kmol / kg bar)	1.0
IP1 Water (kmol/ kg bar)	0.2806
IP2 Nitrogen (1/bar)	1.0
IP2 Water (1/bar)	29.945

Table 24. Values and specifications for the 1st node of the bed

Node Description	**Specification**	**Value**
Mole fraction within first element, Nitrogen (kmol/kmol)	Initial	1.0

Continuation of Table 24.

Mole fraction within first element, Water (kmol/kmol)	Initial	0.0
Solid loading within first element, Nitrogen (kmol/kg)	Rateinitial	0.0
Solid loading within first element, Water (kmol/kg)	Rateinitial	0.0

Table 25 gives the feed specifications for the simulation. The flowrate is kept low according to the bed dimensions. Results are reported for two for different water compositions.

Product specifications are given in Table 26. The outlet flowrate and pressure are dependent upon the pressure dropped inside the bed.

Table 25. Feed specification and values

Description (Units)	**Specification**	**Value/Type**
Model type		Reversible pressure setter
Flowrate (kmol/s)	Fixed	5×10^{-008}
Composition in forward direction, Nitrogen (kmol/kmol)	Fixed	0.95 0.90
Composition in forward direction, Water (kmol/kmol)	Fixed	0.05 0.10
Temperature in forward direction (K)	Fixed	423.15
Boundary pressure (bar)	Fixed	0.1

Table 26. Product specification and values

Description (Units)	**Specification**	**Value/Type**
Model type		Reversible pressure setter
Flowrate (kmol/s)	Free	Pressure drop dependent
Composition in reverse direction, Nitrogen (kmol/kmol)	Fixed	1.0
Composition in reverse direction, Water (kmol/kmol)	Fixed	0.0
Temperature in forward direction (K)	Fixed	423.15
Boundary pressure (bar)	Free	

Figure 42 shows the breakthrough curve for water with 5% composition. Approximately for the first 5000 seconds all the water is adsorbed. At around 5000 seconds a small amount of water starts to come out from the outlet stream, and this is the breakthrough point. At about 12000

seconds it reaches the equilibrium value of 0.05 kmol/kmol. The slope of the curve is gradual which indicates that higher amounts of water can be adsorbed.

Figure 43 shows the breakthrough curve for water with 10% composition. The curve is steeper indicating that larger volume would become difficult to handle. It also indicates that the active sites become saturated much quicker compared to when water was only 5% of the total composition.

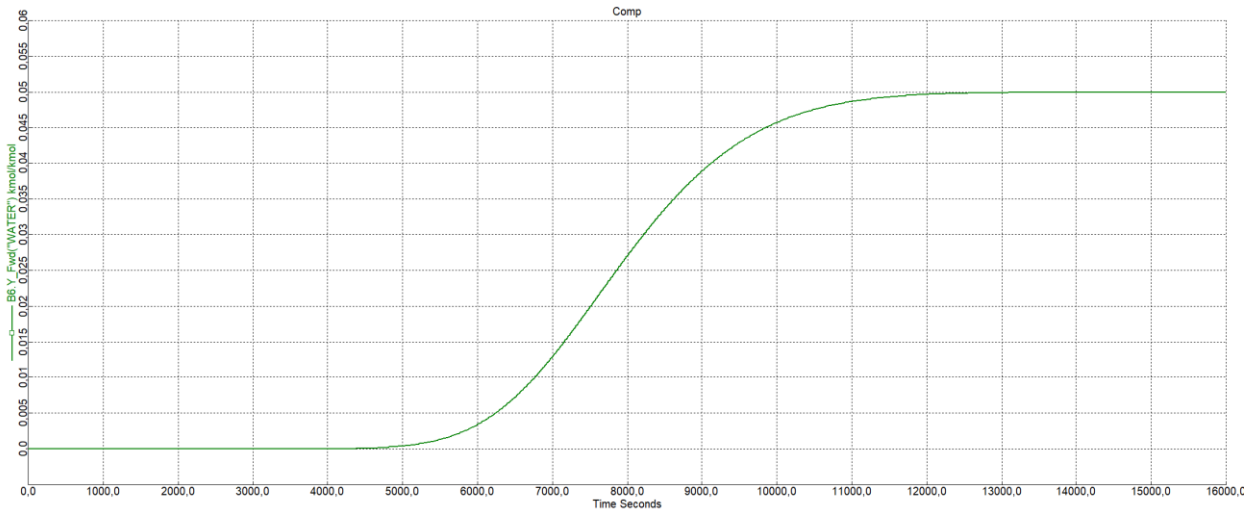

Figure 42. Change in composition of water in product stream with time (when water is 5% of the composition in feed)

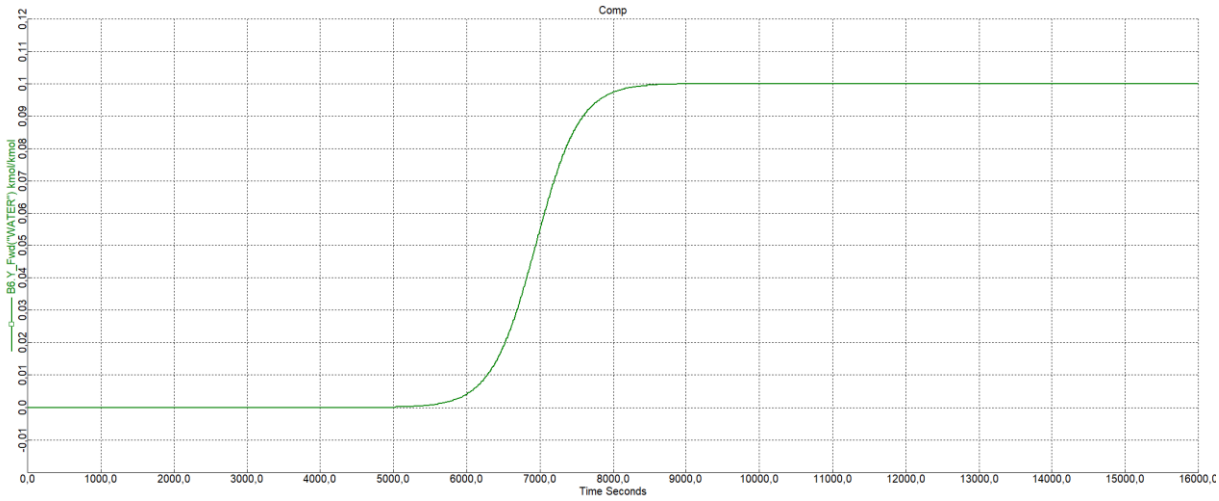

Figure 43. Change in composition of water in product stream with time (when water is 10% of the composition in feed)

Figure 44 shows the water loading at different node positions. The red curve is for the position furthest away in the bed and that is why it reaches the equilibrium value at the last. Dark blue curve is for the fifth node, and it clearly reaches equilibrium before the other node positions. Maximum loading can be noticed as little more than 0.002 kmol/kg.

Referring back to Figure 7 from Wang et al, for temperature of 200 °C, and pressure between 10^{-2} and 10^{-1} bar the loading is approximately between 2 and 4 mol/kg. This is comparative to the value we get from our model, supporting the validity of the model.

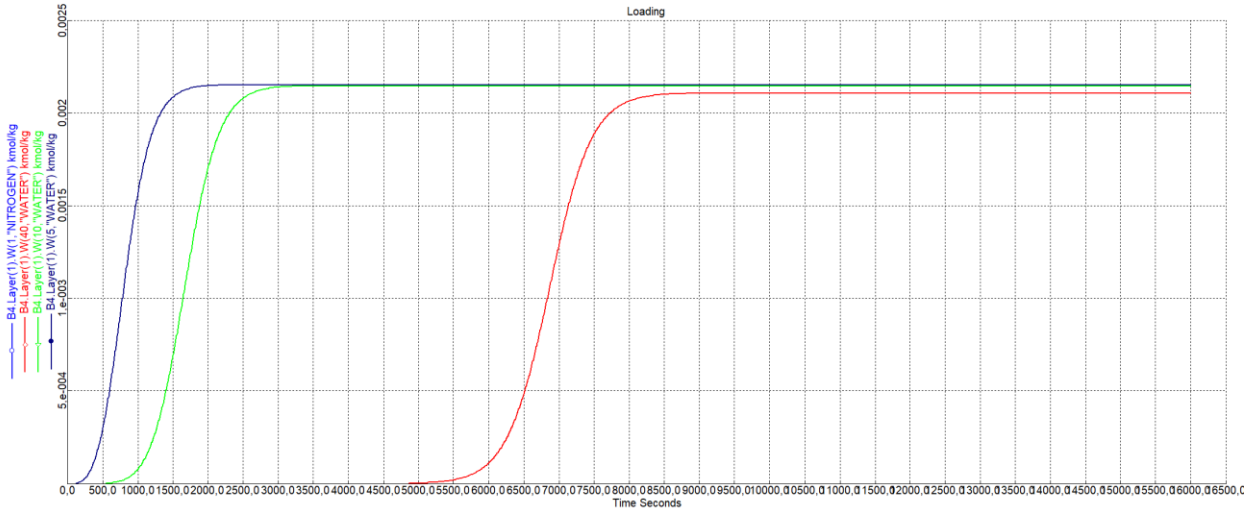

Figure 44. Water loading at different node positions

6 CONCLUSIONS

Gas separation has always been an important research topic in chemical and process industry. Now with the better understanding of the environmental impacts of some of these gases, and their potential as a feedstock, it is even more important to find the right processes for the separation and capture of these gases. Since modelling and simulation is a crucial step before developing the actual process, this work is focused on exploring the potential of Aspen Adsorption® as the useful tool for simulation of adsorption processes.

In the initial stages, effort was made to understand how the software works, and how to use it. The user interface was found to be simple enough for a person with experience of using the other simulation tools. Setting up a flowsheet is straightforward, though extra care is required with choosing the right unit operations and connections. For instance, there are different adsorption columns for the steady state and the dynamic mode.

Governing equations were also studied to better understand the working of the software and to analyze if the results are consistent with the experimental data available. For instance, results of water adsorption were compared to experimental data, and it was found to be consistent with each other.

Modelling of cyclic adsorption process is possible with the Cycle Organizer, which is one of the main advantages of Aspen Adsorption®. Unfortunately, model building with the Cycle Organizer is not straightforward and training and support from the software manufacturer would be very useful to achieve successful simulations. TSA model was successfully made with the software, but certain problems were encountered with a cyclic PSA model, therefore, omitted from this work.

For future, one could work with more complex PSA systems to get a better idea of how the software works in a more practical scenario. It is important to note that only dynamic simulation mode was used for all the simulations, and for future research it could be useful to test the capabilities of the software in the steady state mode.

7 REFERENCES

[1] H. Ritchie and M. Roser, "CO2 and Greenhouse Gas Emissions," 2017. https://ourworldindata.org/co2-and-other-greenhouse-gas-emissions.

[2] P. Morice, C, J. . Kennedy, N. . Rayner, and P. . Jones, "Quantifying uncertainties in global and regional temperature change using an ensemble of observational estimates: The HadCRUT4 dataset," *Geophys. Res.*, vol. 117, 2012, doi: 10.1029/2011JD017187.

[3] IPCC, "Global Warming of 1.5°C. An IPCC Special Report on the impacts of global warming of 1.5°C above pre-industrial levels and related global greenhouse gas emission pathways, in the context of strengthening the global response to the threat of climate change," 2018. [Online]. Available: https://www.ipcc.ch/sr15/.

[4] WWF, "What Are Climate Change and Global Warming?," 2021. https://www.wwf.org.uk/climate-change-and-global-warming.

[5] EPA, "Global Greenhouse Gas Emissions Data," 2020. https://www.epa.gov/ghgemissions/global-greenhouse-gas-emissions-data (accessed Feb. 10, 2021).

[6] R. Lindsey, "Climate Change: Atmospheric Carbon Dioxide," *NOAA*, 2020. https://www.climate.gov/.

[7] C. Song, "Global challenges and strategies for control, conversion and utilization of CO2 for sustainable development involving energy, catalysis, adsorption and chemical processing," *Catal. Today*, vol. 115, no. 1–4, pp. 2–32, 2006, doi: 10.1016/j.cattod.2006.02.029.

[8] N. S. Spinner, J. A. Vega, and W. E. Mustain, "Recent progress in the electrochemical conversion and utilization of CO 2," *Catal. Sci. Technol.*, vol. 2, no. 1, pp. 19–28, 2012, doi: 10.1039/c1cy00314c.

[9] Z. Dehghani, M. Bayat, and M. R. Rahimpour, "Sorption-enhanced methanol synthesis: Dynamic modeling and optimization," *J. Taiwan Inst. Chem. Eng.*, vol. 45, no. 4, pp. 1490–1500, 2014, doi: 10.1016/j.jtice.2013.12.001.

[10] R. Ben-Mansour *et al.*, "Carbon capture by physical adsorption: Materials, experimental investigations and numerical modeling and simulations - A review," *Appl. Energy*, vol. 161, pp. 225–255, 2016, doi: 10.1016/j.apenergy.2015.10.011.

[11] IPCC, "IPCC Special Report on Carbon Dioxide Capture and Storage. Cambridge University Press.," Cambridge, 2005.

[12] S. Z. Saw and J. Nandong, "Simultaneous Carbon Capture and Reuse Using Catalytic Membrane Reactor in Water-Gas Shift Reaction," *Chem. Prod. Process Model.*, vol. 12, no. 4, pp. 1–14, 2017, doi: 10.1515/cppm-2017-0018.

[13] D. Jansen, M. Gazzani, G. Manzolini, E. Van Dijk, and M. Carbo, "Pre-combustion CO2 capture," *Int. J. Greenh. Gas Control*, vol. 40, pp. 167–187, 2015, doi: 10.1016/j.ijggc.2015.05.028.

[14] W. Chen *et al.*, "A new approach to the upgrading of the traditional propylene carbonate washing process with significantly higher CO2 absorption capacity and selectivity," *Appl. Energy*, vol. 240, no. February, pp. 265–275, 2019, doi: 10.1016/j.apenergy.2019.01.236.

[15] Z. H. Ban, L. K. Keong, and A. M. Shariff, "Physical absorption of CO2 capture: A review," *Adv. Mater. Res.*, vol. 917, pp. 134–143, 2014, doi: 10.4028/www.scientific.net/AMR.917.134.

[16] C. H. Yu, C. H. Huang, and C. S. Tan, "A review of CO2 capture by absorption and adsorption," *Aerosol Air Qual. Res.*, vol. 12, no. 5, pp. 745–769, 2012, doi: 10.4209/aaqr.2012.05.0132.

[17] S. Valluri and S. K. Kawatra, "Simultaneous removal of CO2, NOx and SOx using single stage absorption column," *J. Environ. Sci. (China)*, vol. 103, no. x, pp. 279–287, 2021, doi: 10.1016/j.jes.2020.11.006.

[18] I. P. Koronaki, L. Prentza, and V. Papaefthimiou, "Modeling of CO2 capture via chemical absorption processes - An extensive literature review," *Renew. Sustain. Energy Rev.*, vol. 50, pp. 547–566, 2015, doi: 10.1016/j.rser.2015.04.124.

[19] M. Wang, A. Lawal, P. Stephenson, J. Sidders, and C. Ramshaw, "Post-combustion CO2 capture with chemical absorption: A state-of-the-art review," *Chem. Eng. Res. Des.*, vol. 89, no. 9, pp. 1609–1624, 2011, doi: 10.1016/j.cherd.2010.11.005.

[20] A. F. Ismail, K. C. Khulbe, and T. Matsuura, *Gas separation membranes: Polymeric and inorganic*. 2015.

[21] A. Brunetti, F. Scura, G. Barbieri, and E. Drioli, "Membrane technologies for CO2 separation," *J. Memb. Sci.*, vol. 359, no. 1–2, pp. 115–125, 2010, doi: 10.1016/j.memsci.2009.11.040.

[22] G. Clarizia and P. Bernardo, "30 years of membrane technology for gas separation," *Chem Eng Trans*, vol. 32, no. 1994–2004, 2013.

[23] E. Drioli, A. Brunetti, and G. Barbieri, "Ceramic Membranes in Carbon Dioxide Capture: Applications and Potentialities," *Adv. Sci. Technol.*, vol. 72, pp. 105–118, 2010, doi: 10.4028/www.scientific.net/ast.72.105.

[24] S. Alexander Stern, "Polymers for gas separations: the next decade," *J. Memb. Sci.*, vol. 94, no. 1, pp. 1–65, 1994, doi: 10.1016/0376-7388(94)00141-3.

[25] M. J and F. M, "CO2 Separation from Flue Gases Using Different Types of Membranes," *J. Membr. Sci. Technol.*, vol. 6, no. 2, 2016, doi: 10.4172/2155-9589.1000153.

[26] G. Xu, F. Liang, Y. Yang, Y. Hu, K. Zhang, and W. Liu, "An improved CO2 separation and purification system based on cryogenic separation and distillation theory," *Energies*, vol. 7, no. 5, pp. 3484–3502, 2014, doi: 10.3390/en7053484.

[27] J. . Seader, J. E. Henley, and D. K. Roper, *Separation Process Principles: Chemical and Biochemical Operations*, 3rd ed. John Wiley & Sons, Inc., 2011.

[28] D. M. D'Alessandro, B. Smit, and J. R. Long, "Carbon dioxide capture: Prospects for new materials," *Angew. Chemie - Int. Ed.*, vol. 49, no. 35, pp. 6058–6082, 2010, doi: 10.1002/anie.201000431.

[29] E. Knapik, P. Kosowski, and J. Stopa, "Cryogenic liquefaction and separation of CO2 using nitrogen removal unit cold energy," *Chem. Eng. Res. Des.*, vol. 131, pp. 66–79, 2018, doi: 10.1016/j.cherd.2017.12.027.

[30] T. L. P. Dantas *et al.*, "Carbon dioxide-nitrogen separation through adsorption on activated carbon in a fixed bed," *Chem. Eng. J.*, vol. 169, no. 1–3, pp. 11–19, 2011, doi: 10.1016/j.cej.2010.08.026.

[31] D. Do, Duong, *Adsorption Analysis: Equilibria and Kinetics*. London: Imperial College Press, 1998.

[32] N. P. Wickramaratne and M. Jaroniec, "Activated carbon spheres for CO2 adsorption," *ACS Appl. Mater. Interfaces*, vol. 5, no. 5, pp. 1849–1855, 2013, doi: 10.1021/am400112m.

[33] S. W. Choi, J. Tang, V. G. Pol, and K. B. Lee, "Pollen-derived porous carbon by KOH activation: Effect of physicochemical structure on CO 2 adsorption," *J. CO2 Util.*, vol. 29, no. November 2018, pp. 146–155, 2019, doi: 10.1016/j.jcou.2018.12.005.

[34] B. J. Lee, J. Kim, and T. Hyeon, "Recent Progress in the Synthesis of Porous Carbon Materials **," *Adv. Mater.*, vol. 18, pp. 2073–2094, 2006, doi: 10.1002/adma.200501576.

[35] D. D. Do and K. Words-coal, "THE PREPARATION OF ACTIVE CARBONS FROM COAL BY CHEMICAL AND PHYSICAL ACTIVATION," vol. 34, no. 4, pp. 471–479, 1996.

[36] D. Bonenfant, M. Kharoune, P. Niquette, M. Mimeault, and R. Hausler, "Advances in principal factors influencing carbon dioxide adsorption on zeolites," *Sci. Technol. Adv. Mater.*, vol. 9, no. 013007, 2008, doi: 10.1088/1468-6996/9/1/013007.

[37] R. V. Siriwardane, M. S. Shen, E. P. Fisher, and J. Losch, "Adsorption of CO2 on zeolites at moderate temperatures," *Energy and Fuels*, vol. 19, no. 3, pp. 1153–1159, 2005, doi: 10.1021/ef040059h.

[38] Y. Guo, H. Zhang, and Y. Liu, "Desorption characteristics and kinetic parameters determination of molecular sieve by thermogravimetric analysis/differential thermogravimetric analysis technique," *Adsorpt. Sci. Technol.*, vol. 36, no. 7–8, pp. 1389–1404, 2018, doi: 10.1177/0263617418772665.

[39] E. Jaramillo and M. Chandross, "Adsorption of Small Molecules in LTA Zeolites. 1. NH 3 , CO 2 , and H 2 O in Zeolite 4A," *J. Phys. Chem. B*, vol. 108, no. 52, pp. 20155–20159, 2004.

[40] J. R. Li *et al.*, "Carbon dioxide capture-related gas adsorption and separation in metal-organic frameworks," *Coord. Chem. Rev.*, vol. 255, no. 15–16, pp. 1791–1823, 2011, doi: 10.1016/j.ccr.2011.02.012.

[41] J. Liu, P. K. Thallapally, B. P. Mc Grail, D. R. Brown, and J. Liu, “Progress in adsorption-based CO2 capture by metal–organic frameworks,” *Chem. Soc. Rev.*, vol. 41, no. 6, pp. 2308–2322, 2012, doi: 10.1039/c1cs15221a.

[42] H. Furukawa *et al.*, “Ultrahigh Porosity in Metal-Organic Frameworks,” *Science (80-.).*, vol. 329, no. July, pp. 424–429, 2010.

[43] A. Hanif, S. Dasgupta, S. Divekar, A. Arya, M. O. Garg, and A. Nanoti, “A study on high temperature CO 2 capture by improved hydrotalcite sorbents,” *Chem. Eng. J.*, vol. 236, pp. 91–99, 2014, doi: 10.1016/j.cej.2013.09.076.

[44] D. G. Cantrell, L. J. Gillie, A. F. Lee, and K. Wilson, “Structure-reactivity correlations in MgAl hydrotalcite catalysts for biodiesel synthesis,” *Appl. Catal. A Gen.*, vol. 287, no. 2, pp. 183–190, 2005, doi: 10.1016/j.apcata.2005.03.027.

[45] N. Ayawei, A. N. Ebelegi, and D. Wankasi, “Modelling and Interpretation of Adsorption Isotherms,” *J. Chem.*, vol. 2017, no. 3039817, 11, 2017, doi: 10.1155/2017/3039817.

[46] Y. Liu, “Some consideration on the Langmuir isotherm equation,” *Colloids Surfaces A Physicochem. Eng. Asp.*, vol. 274, pp. 34–36, 2006, doi: 10.1016/j.colsurfa.2005.08.029.

[47] P. Schneider, “Adsorption isotherms of microporous-mesoporous solids revisited,” *Appl. Catal. A Gen.*, vol. 129, no. 95, pp. 157–165, 1995.

[48] K. R. Wood, Y. A. Liu, and Y. Yu, “Simulation of Adsorption Processes,” in *Design, Simulation, and Optimization of Adsorptive and Chromatographic Separations: A Hands-On Approach*, Wiley-VCH Verlag GmbH & Co. KGaA, 2018.

[49] K. S. . Sing *et al.*, “Reporting physisorption data for gas/solid systems with special reference to the determination of surface area and porosity (Recommendations 1984),” *Pure Appl. Chem*, vol. 57, no. 4, pp. 603–619, 1985.

[50] M. Muttakin, S. Mitra, K. Thu, K. Ito, and B. Baran, “International Journal of Heat and Mass Transfer Theoretical framework to evaluate minimum desorption temperature for IUPAC classified adsorption isotherms,” *Int. J. Heat Mass Transf.*, vol. 122, pp. 795–805, 2018, doi: 10.1016/j.ijheatmasstransfer.2018.01.107.

[51] K. D. Hammond and W. C. Conner, “Analysis of catalyst surface structure by physical sorption,” in *Advances in Catalysis*, vol. 56, Academic Press Inc., 2013, pp. 1–101.

[52] O. Sahu and N. Singh, “Significance of bioadsorption process on textile industry wastewater,” in *The Impact and Prospects of Green Chemistry for Textile Technology*, Elsevier, 2018, pp. 367–416.

[53] AspenTech, “Aspen Adsoprtion Help,” Bedford, 2019.

[54] J. S. Piccin, T. R. S. A. Cadaval, L. A. A. De Pinto, and G. L. Dotto, *Adsorption isotherms in liquid phase: Experimental, modeling, and interpretations*. 2017.

[55] L. D. Gelb and K. E. Gubbins, “Characterization of Porous Glasses : Simulation Models , Adsorption Isotherms , and the Brunauer - Emmett - Teller Analysis Method,”

Langmuir, vol. 14, no. 8, pp. 2097–2111, 1998.

[56] S. Jribi *et al.*, "Equilibrium and kinetics of CO2 adsorption onto activated carbon," *Int. J. Heat Mass Transf.*, vol. 108, pp. 1941–1946, 2017, doi: 10.1016/j.ijheatmasstransfer.2016.12.114.

[57] Y. Wang, "Measurements and Modeling of Water Adsorption Isotherms of Zeolite Linde-Type A Crystals," *Ind. Eng. Chem. Res.*, vol. 59, pp. 8304–8314, 2020, doi: 10.1021/acs.iecr.9b06891.

[58] R. Lin, J. Liu, Y. Nan, D. W. Depaoli, and L. L. Tavlarides, "Kinetics of Water Vapor Adsorption on Single-Layer Molecular Sieve 3A : Experiments and Modeling," *Ind. Eng. Chem. Res.*, vol. 53, pp. 16015–16024, 2014.

[59] A. Belloni, "Adsorption – a Successful and Versatile Separation Technique Continuously Improved at Linde," *Chemie Ing. Tech.*, vol. 83, no. I–2, pp. 29–35, 2011, doi: 10.1002/cite.201000150.

[60] B. Crittenden and J. Thomas, W, *Adsorption technology and design*. Oxford: Butterworth-Heinemann, 1998.

[61] J. A. Mason, K. Sumida, Z. R. Herm, R. Krishna, and J. R. Long, "Evaluating metal-organic frameworks for post-combustion carbon dioxide capture via temperature swing adsorption," *Energy Environ. Sci.*, vol. 4, no. 8, pp. 3030–3040, 2011, doi: 10.1039/c1ee01720a.

[62] L. Riboldi and O. Bolland, "Overview on Pressure Swing Adsorption (PSA) as CO2 Capture Technology: State-of-the-Art, Limits and Potentials," *Energy Procedia*, vol. 114, no. 1876, pp. 2390–2400, 2017, doi: 10.1016/j.egypro.2017.03.1385.

[63] N. Hedin, L. Andersson, L. Bergström, and J. Yan, "Adsorbents for the post-combustion capture of CO2 using rapid temperature swing or vacuum swing adsorption," *Appl. Energy*, vol. 104, pp. 418–433, 2013, doi: 10.1016/j.apenergy.2012.11.034.

[64] M. T. Ho, G. W. Allinson, and D. E. Wiley, "Reducing the cost of CO2 capture from flue gases using pressure swing adsorption," *Ind. Eng. Chem. Res.*, vol. 47, no. 14, pp. 4883–4890, 2008, doi: 10.1021/ie070831e.

[65] S. Cavenati, C. A. Grande, and A. E. Rodrigues, "Removal of carbon dioxide from natural gas by vacuum pressure swing adsorption," *Energy and Fuels*, vol. 20, no. 6, pp. 2648–2659, 2006, doi: 10.1021/ef060119e.

[66] S. Hayashi, H. Tsuchiya, and K. Haruna, "Process for obtaining high concentration argon by pressure-swing-adsorption," 4,529,412, 1985.

[67] M. M. A. Mendes, C. A. V Costa, and A. E. Rodrigues, "Oxygen separation from air by PSA : modelling and experimental results Part I : isothermal operation," *Sep. Purif. Technol.*, vol. 24, pp. 173–188, 2001.

[68] J. Bonjour, J. B. Chalfen, and F. Meunier, "Temperature swing adsorption process with indirect cooling and heating," *Ind. Eng. Chem. Res.*, vol. 41, no. 23, pp. 5802–5811, 2002,

doi: 10.1021/ie011011j.

[69] K. Z. House, C. F. Harvey, J. Aziz, and D. P. Schrag, “The energy penalty of post-combustion CO 2 capture & storage and its implications for retrofitting the U . S . installed base,” pp. 193–205, 2009, doi: 10.1039/b811608c.

[70] T. D. Burchell, R. R. Judkins, M. R. Rogers, and A. M. Williams, “A NOVEL PROCESS AND MATERIAL FOR THE SEPARATION OF CARBON DIOXIDE AND HYDROGEN SULFIDE GAS MIXTURES,” *Carbon N. Y.*, vol. 35, no. 9, pp. 1279–1294, 1997.

[71] C. A. Grande, R. P. L. Ribeiro, E. L. G. Oliveira, and A. E. Rodrigues, “Electric swing adsorption as emerging CO2 capture technique,” *Energy Procedia*, vol. 1, no. 1, pp. 1219–1225, 2009, doi: 10.1016/j.egypro.2009.01.160.

[72] V. Tartaglione, C. Farges, and J. Sabatier, “Nonlinear dynamical modeling of adsorption and desorption processes with power-law kinetics: Application to CO2 capture,” *Phys. Rev. E*, vol. 102, no. 5, pp. 1–10, 2020, doi: 10.1103/PhysRevE.102.052102.

[73] A. Seidel-Morgenstern, “Experimental determination of single solute and competitive adsorption isotherms,” *J. Chromatogr. A*, vol. 1037, no. 1–2, pp. 255–272, 2004, doi: 10.1016/j.chroma.2003.11.108.

[74] W. J. Weber and E. H. Smith, “Simulation and design models for adsorption processes,” *Environ. Sci. Technol.*, vol. 21, no. 11, pp. 1040–1050, 1987, doi: 10.1021/es00164a002.

[75] M. F. Edwards and J. F. Richardson, “Gas dispersion in packed beds,” *Chem. Eng. Sci.*, vol. 23, no. 2, pp. 109–123, 1968, doi: 10.1016/0009-2509(68)87056-3.

[76] H. R. Sant Anna, A. G. Barreto, F. W. Tavares, and M. B. de Souza, “Machine learning model and optimization of a PSA unit for methane-nitrogen separation,” *Comput. Chem. Eng.*, vol. 104, pp. 377–391, 2017, doi: 10.1016/j.compchemeng.2017.05.006.

[77] E. Gleuckauf and J. I. Coates, “Theory of Chromatography. Part IV. The Influence of Incomplete Equilibrium on the Front Boundary of Chromatograms and on the Effectiveness of Separation,” *J. Chem. Soc*, vol. 0, pp. 1315–1321, 1947.

[78] A. Dabrowski, “Adsorption - from theory to practice ,” *Adv. Colloid Interface Sci.*, vol. 93, pp. 135–224, 2001.

[79] Honeywell International Inc, “Aromatics/Sorbex Separation,” 2021. https://honeywell-uop.azurewebsites.net/equipment/aromatics-separation/ (accessed Mar. 26, 2021).

[80] Durr Systems Inc, “Solvent Recovery Adsorption and Distillation Systems,” 2020. https://www.durr-megtec.com/.

[81] P. O. J. Scherer, “Discretization of Differential Equations,” in *Computational Physics, Graduate Texts in Physics*, Springer International Publishing AG, 2017, pp. 255–287.

[82] C. Tian, Q. Fu, Z. Ding, Z. Han, and D. Zhang, “Experiment and simulation study of a dual-reflux pressure swing adsorption process for separating N 2 / O 2,” *Sep. Purif.*

Technol., vol. 189, pp. 54–65, 2017, doi: 10.1016/j.seppur.2017.06.041.

[83] Y. Tavan, “Aspen Adsorption Training CO2,” 2020. https://www.youtube.com/watch?v=Vj3n_dUJ3Vo.

Appendix I

Tables I1 and I2 [58] gives us the experimental adsorption data for H_2O on zeolite 3A crystal adsorbent at different temperatures.

Table I1. Experimental data for H_20 at 25, 50 and 100 °C

T = 25 °C		**T = 50 °C**		**T = 100 °C**	
p (bar)	q(mol/kg)	p (bar)	q(mol/kg)	p (bar)	q(mol/kg)
1.0×10^{-5}	3.36	1.0×10^{-5}	1.41	9.0×10^{-5}	1.18
2.0×10^{-5}	4.79	2.0×10^{-5}	1.82	1.0×10^{-4}	1.63
5.0×10^{-5}	7.60	5.0×10^{-5}	2.76	5.0×10^{-4}	2.23
1.0×10^{-4}	8.70	1.0×10^{-4}	4.30	1.0×10^{-3}	3.09
2.0×10^{-4}	9.34	2.0×10^{-4}	6.32	3.0×10^{-3}	5.39
5.0×10^{-4}	10.01	5.0×10^{-4}	8.31	5.0×10^{-3}	6.79
1.0×10^{-3}	10.50	1.0×10^{-3}	9.12	9.9×10^{-3}	8.18
3.0×10^{-3}	11.24	3.0×10^{-3}	10.03	2.0×10^{-2}	9.10
5.0×10^{-3}	11.64	5.0×10^{-3}	10.42	3.0×10^{-2}	9.54
9.9×10^{-3}	12.17	1.0×10^{-2}	10.96	4.0×10^{-2}	9.83
2.0×10^{-2}	12.71	2.0×10^{-2}	11.51		
2.5×10^{-2}	12.96	2.5×10^{-2}	11.70		

Table I2. Experimental data for H_20 at 150 and 200 °C

T = 150 °C		**T = 200 °C**	
p (bar)	q(mol/kg)	p (bar)	q(mol/kg)
1.0×10^{-4}	0.24	1.0×10^{-4}	0.17
2.0×10^{-4}	0.51	2.0×10^{-4}	0.23
$5.0 \times 10\text{-}^{4}$	0.84	5.0×10^{-4}	0.39
1.0×10^{-3}	1.14	9.9×10^{-4}	0.55
3.0×10^{-3}	1.86	3.0×10^{-3}	0.87
3.3×10^{-3}	1.97	5.0×10^{-3}	1.06
5.0×10^{-3}	2.40	9.7×10^{-3}	1.39

Continuation of Table I2.

5.4×10^{-3}	2.29	2.0×10^{-2}	1.90
1.0×10^{-2}	3.25	3.0×10^{-2}	2.29
2.0×10^{-2}	4.41	4.0×10^{-2}	2.65
3.0×10^{-2}	5.51		
4.0×10^{-2}	6.33		

Tables I3 and I4 [58] gives us the experimental adsorption data for H_2O on zeolite 4A crystal adsorbent at different temperatures.

Table I3. Experimental data for H_20 at 25, 50 and 100 °C

T = 25 °C		**T = 50 °C**		**T = 100 °C**	
p (bar)	q(mol/kg)	p (bar)	q (mol/kg)	p (bar)	q(mol/kg)
1.0×10^{-5}	3.78	2.0×10^{-5}	2.65	2.0×10^{-5}	2.09
2.0×10^{-5}	5.08	5.0×10^{-5}	3.22	5.0×10^{-5}	2.20
5.0×10^{-5}	8.70	8.0×10^{-5}	3.79	1.0×10^{-4}	2.25
8.0×10^{-5}	10.09	1.0×10^{-4}	4.20	2.0×10^{-4}	2.44
1.0×10^{-4}	10.51	2.0×10^{-4}	6.17	5.0×10^{-4}	2.92
2.0×10^{-4}	11.36	5.0×10^{-4}	9.68	8.0×10^{-4}	3.36
5.0×10^{-4}	12.15	8.0×10^{-4}	10.63	1.0×10^{-3}	3.61
8.0×10^{-4}	12.48	1.0×10^{-3}	10.93	3.0×10^{-3}	5.84
1.0×10^{-3}	12.62	3.0×10^{-3}	11.93	5.0×10^{-3}	7.61
3.0×10^{-3}	13.30	5.0×10^{-3}	12.34	8.0×10^{-3}	9.14
5.0×10^{-3}	13.63	8.0×10^{-3}	12.70	1.1×10^{-2}	9.84
8.0×10^{-3}	13.95	1.1×10^{-2}	12.92	1.5×10^{-2}	10.45
1.1×10^{-2}	14.17	1.5×10^{-2}	13.16	2.0×10^{-2}	10.88
1.5×10^{-2}	14.40	2.0×10^{-2}	13.38	2.5×10^{-2}	11.16
2.0×10^{-2}	14.62	2.5×10^{-2}	13.54		
2.5×10^{-2}	14.82				

Table I4. Experimental data for H_20 at 200 and 250 °C

T = 200 °C		**T = 250 °C**	
p (bar)	q(mol/kg)	p (bar)	q(mol/kg)
2.0×10^{-5}	1.11	1.0×10^{-4}	0.90
5.0×10^{-5}	1.31	2.0×10^{-4}	0.99
8.0×10^{-5}	1.36	5.0×10^{-4}	1.11
1.0×10^{-4}	1.37	8.0×10^{-4}	1.20
2.0×10^{-4}	1.40	1.0×10^{-3}	1.24
5.0×10^{-4}	1.51	3.0×10^{-3}	1.51
8.0×10^{-4}	1.61	5.0×10^{-3}	1.65
1.0×10^{-3}	1.67	8.0×10^{-3}	1.78
3.0×10^{-3}	1.97	1.1×10^{-2}	1.88
5.0×10^{-3}	2.15	1.5×10^{-2}	1.97
8.0×10^{-3}	2.34	2.0×10^{-2}	2.07
1.1×10^{-2}	2.47	2.5×10^{-2}	2.15
1.5×10^{-2}	2.63		
2.0×10^{-2}	2.80		
2.5×10^{-2}	2.95		

Table I5 gives us the experimental adsorption data for CO_2 at different temperatures.

Table I5. Experimental data for CO2 at 0, 30 and 70 °C

T = 0 °C		**T = 30 °C**		**T = 70 °C**	
p (bar)	q(mol/kg)	p (bar)	q(mol/kg)	p (bar)	q(mol/kg)
2.6×10^{-7}	2.2	1.28×10^{-7}	1.30	2.95×10^{-7}	0.71
1.89×10^{-6}	2.82	3.85×10^{-7}	1.67	9.92×10^{-7}	1.02
1.08×10^{-5}	4.08	1.34×10^{-6}	1.93	4.35×10^{-6}	1.49
4.72×10^{-5}	8.28	4.35×10^{-6}	2.22	1.16×10^{-5}	1.70
1.92×10^{-4}	16.8	1.83×10^{-5}	2.78	3.49×10^{-5}	1.95
4.58×10^{-4}	23.9	8.66×10^{-5}	3.97	7.44×10^{-5}	2.22
1.73×10^{-3}	35.1	3.65×10^{-4}	8.28	2.23×10^{-4}	2.74
7.56×10^{-3}	52.1	6.69×10^{-4}	11.1	8.09×10^{-4}	3.75
2.1×10^{-2}	70.2	1.86×10^{-3}	17.0	1.86×10^{-3}	5.34

Continuation table I5.

5.2×10^{-2}	85.6	5.58×10^{-3}	26.1	3.41×10^{-3}	7.60
1.15×10^{-2}	95.8	2.18×10^{-2}	42.8	8.74×10^{-3}	12.7
1.89×10^{-1}	100	5.41×10^{-2}	57.6	3.31×10^{-2}	24.6
		1.07×10^{-1}	68.2	1.34×10^{-1}	44.0
		5.88×10^{-1}	97.2	1.0	82.0